

Cepheid Calibration of the Peak Brightness of SNe Ia.

XI. SN 1998aq in NGC 3982

A. Saha

National Optical Astronomy Observatories
950 North Cherry Ave., Tucson, AZ 85726

Allan Sandage

The Observatories of the Carnegie Institution of Washington
813 Santa Barbara Street, Pasadena, CA 91101

G. A. Tammann

Astronomisches Institut der Universität Basel
Venusstrasse 7, CH-4102 Binningen, Switzerland

A. E. Dolphin, J. Christensen

National Optical Astronomy Observatories
950 North Cherry Ave., Tucson, AZ 85726

and

N. Panagia¹, F.D. Macchetto¹

Space Telescope Science Institute
3700 San Martin Drive, Baltimore, MD 21218

Received _____; accepted _____

Submitted to the Astrophysical Journal, Part I

¹Affiliated to the Astrophysics Division, Space Sciences Department of ESA.

ABSTRACT

Repeated imaging observations have been made of NGC 3982 with the *Hubble Space Telescope* between March and May 2000, over an interval of 53 days. Images were obtained on 12 epochs in the *F555W* band and on five epochs in the *F814W* band. The galaxy hosted the type Ia supernova SN1998aq.

A total of 26 Cepheid candidates were identified, with periods ranging from 10 to 45 days, using photometry with the DoPHOT program. The de-reddened distance to NGC 3982 is estimated from these data using various criteria to maximize signal to noise and reliability: the values lie between 31.71 and 31.82, with uncertainties in the mean of typically ± 0.14 mag for each case. A parallel analysis using photometry with HSTphot discovered 13 variables, yielding a distance modulus of 31.85 ± 0.16 . The final adopted modulus is $(M - m)_0 = 31.72 \pm 0.14$ (22 ± 1.5 Mpc).

Photometry of 1998aq that is available in the literature is used in combination with the derived distance to NGC 3982 to obtain the peak absolute magnitude of this supernova. The lower limit (no extinction within the host galaxy) for M_V is -19.47 ± 0.15 mag. Corrections for decline rate and intrinsic color to carry these to the reduced system of Parodi et al. (2000) have been performed. The derived luminosities at hand are fully consistent with the mean of the 8 normal SNe Ia previously calibrated with Cepheids. Together they yield $H_0 \approx 60 \pm 2(\text{internal}) \text{ km s}^{-1} \text{ Mpc}^{-1}$ based on an assumed LMC distance modulus of 18.50. We point out that correcting some of the systematic errors and including uncertainty estimates due to them leads to $H_0 = 58.7 \pm 6.3(\text{internal}) \text{ km s}^{-1} \text{ Mpc}^{-1}$.

Subject headings: Cepheids — distance scale — galaxies: individual (NGC 3982)

— supernovae: individual (SN 1998aq)

1. Introduction

This is the eleventh paper of a series whose purpose is to obtain Cepheid distances to galaxies that have produced supernovae of type Ia (SNe Ia), thereby calibrating their absolute magnitudes at maximum light. The Hubble diagram for SNe Ia shows a dispersion (read as magnitude residuals about a line of slope $dM/d\log cz = 5$) of less than 0.2 mag when certain second-parameter corrections are applied (Hamuy et al. 1996a, 1996b; Tripp 1998; Phillips et al. 1999; Saha et al. 1999; Tripp & Branch 1999; Parodi et al. 2000; Tammann, Sandage & Saha 2001), the far-field value of the Hubble constant is determined directly from the SNe Ia Hubble diagram once the mean absolute magnitude of SNe Ia at maximum light is calibrated. Clearly the resulting Hubble constant is the global value, free from all local velocity anomalies.

This route to H_0 through Branch-normal SNeIa (Branch et al. 1993; Branch 2001) is the only method that in a *single step* directly bridges the relatively nearby distances from Cepheids with distances well beyond those corresponding to recession velocities of 10,000 km s⁻¹. Such large distances are required for the determination of the *cosmic* value of H_0 , so that the effect of streaming motions is minimized. Magnitude residuals of less than 0.2 mag rms in the Hubble diagram show that Branch-normal SNeIa, once they are corrected for variations in decline rate and intrinsic color, are the best known standard candles. However, before the advent of the *Hubble Space Telescope (HST)*, one had to rely on other secondary distance indicators to obtain the luminosity calibration of SNeIa (Sandage & Tammann 1982), since the nearest galaxies that had hosted recorded SNeIa were beyond the range of ground based Cepheid searches. With the use of *HST*, this step of using intermediate secondary distance indicators has been eliminated. As of this eleventh paper in our series, the peak luminosities of nine Branch-normal SNeIa are now directly tied to Cepheids. For these reasons we claim that the resulting value of H_0 is the cleanest

and most direct of all the ones using the distance ladder methodology.

The Branch normal type Ia SN 1998aq was discovered by M. Armstrong (Hurst 1998) on 1998 April 13, six days before maximum light (see §5). It appeared 18" west and 7" north of the center of NGC 3982, which is a galaxy in the very busy region of the supergalactic plane in what was originally called the Ursa Major cloud (Humason et al. 1956, Table I). The region was later mapped into separate groups by many cartographers. The most complete mapping has been done by Tully (1987), who is the leading student of groups. He also summarized much of the earlier work, principally by de Vaucouleurs (1975). Later work by Nolthenius (1993) on groups is also particularly important to cite.

What is now called the Ursa Major Cluster is in the midst of the Ursa Major Cloud (see map 15 of the Tully-Fisher Atlas, 1987). The most convincing mapping of the region, and the separation of the Ursa Major Cluster from the Cloud, is by Tully et al. (1996). following the thesis of Verheijen (1997). NGC 3982 lies near the extreme northern border of the Cluster as delineated by Verheijen and by Tully et al. (1996). The galaxy is listed in the RSA (Sandage & Tammann 1987) as of type Sbc(r)II-III with a total blue apparent magnitude, corrected for Galactic and internal absorption, of $B_T^{b,i} = 11.59$. Tully lists the apparent magnitude, similarly corrected by his absorption precepts, as $B_T^{b,i} = 11.7$. A color image of this galaxy, created from the the HST V and I band images presented in this paper, is shown in Fig. 1.

Membership in the the Ursa Major Cluster is of no importance in calibrating the absolute magnitude at maximum of its daughter supernova, which is the object of this paper. Nevertheless, our determination of the distance to the galaxy in §4, does, of course, have relevance for comparing the distance to the Ursa Major Cluster summarized by Tully et al. (1996) to be 15.5 Mpc from other methods. This distance, along with their quoted distances of 15.6 Mpc for the Virgo cluster and 14.5 Mpc for the Fornax cluster, defines

their short distance scale leading to their high value of $H_0 = 80$ (Pierce & Tully 1988). Our distance to NGC 3982 from Cepheids (§4 of this paper) is 22.1 Mpc. Combined with the apparent magnitude at maximum of SN 1998aq and the absolute magnitudes at maximum light from eight previous SNe Ia calibrators (Saha et al. 1999; Parodi et al. 2000) leads us again to $H_0 = 59 \pm 6 \text{ km s}^{-1} \text{ Mpc}^{-1}$.

The plan of this paper is as follows. The HST observations of NGC 3982 are set out in §2. Discovery and photometry of the Cepheids is described in §3. The P-L relation and the resulting determination of the apparent as well as absorption-corrected distance moduli are in §4. Discussion of the available photometric data for SN 1998aq and the resulting calibration of its absolute magnitude is in §5. In §6 we compare $M(max)$ for SN 1998aq with the previously calibrated nine SNe Ia, leading to our determination of H_0 using the supernova route.

2. Observations

Repeated images of a field that contains the entire visible region of the galaxy NGC 3982 were obtained using the WFPC2 (Holtzman et al. 1995a) on the *HST* over a 53 day period from 2000 March to May (HST observing program number 8100). The visible galaxy fits within the field of view of the WFPC2, and a composite image including all four chips of the instrument is shown in Fig. 1. Observations were made at 12 discrete epochs in *F555W* passband, and at 5 epochs in the *F814W* passband over the 53 day window. Each epoch in each filter consists of 2 one-orbit duration exposures taken on successive orbits of the spacecraft. This allows the removal of cosmic rays by an anti-coincidence technique described by Saha et al. 1996a (Paper V). The journal of observations is given in Table 1. All exposures in this table are pairs of exposures on back to back space-craft orbits, each of 2500s duration.

EDITOR: PLACE TABLE 1 HERE.

The epochs were spaced strategically over the total duration to provide maximum leverage on detecting and finding periods of Cepheid variables over the period range from 10 to 50 days. It should be remarked that it is highly desirable to keep all the observations at very nearly the same pointing as possible. We have managed to do this in the previous galaxies studied in this series. Due to a combination of a lack of guide stars for this field at some spacecraft roll angles and the pointing constraints posed by the requirements for the solar panels, a large enough window for keeping the pointing orientation unchanged was not available in the present case. Consequently, while the final 11 epochs are all obtained with essentially the same pointing (to within a few pixels), the very first epoch (*F555W* filter only) has a field orientation that is 12 degrees different from the remaining observations.

3. Photometry

3.1. DoPHOT based analysis

The procedural details for processing images, combining the sub-exposures for each epoch while removing the bulk of the cosmic rays, as well as performing the photometry with a variant of DoPHOT (Schechter et al. 1993) optimized for WFPC2 data has been given in Paper V. A subsequent improvement in deriving aperture corrections was detailed in Saha et al. 1999 (Paper IX). Since the same procedures were followed here, the details are not repeated.

3.1.1. A note on magnitude zero points

In keeping with the precepts mentioned in Paper V, measurements in any one passband are expressed in the magnitude system defined by Holtzman et al. (1995b) that is natural to the HST. Specifically we mean the $F555W$ and $F814W$ “ground system” magnitudes. These calibrations were made with “short” exposures, which have since been shown to suffer from the effects of anomalous charge transfer in the CCD devices used (e.g. Whitmore, Heyer & Casertano 1999). It is recognized that the effect of adopting the Holtzman et al. (1995b) calibrations over-estimates the brightness by a few hundredths of a magnitude. In our previous papers of this series, we made a correction of 0.05 mag to both passbands to account for this effect. Our current understanding of this situation is that the exact correction is procedure dependent (Saha et al. 2000). In addition, the charge transfer anomaly has been shown to worsen with time due to exposure to radiation. Thus the exact corrections depend additionally on when a particular data-set was obtained. While Saha et al. 2000 evaluated the appropriate corrections for short exposure data taken in late 1997, that analysis does not directly predict the corrections appropriate for the Holtzman et al. (1995b) calibration. The results of the bright star monitoring program indicate that the deterioration from 1994 to 1997 are unlikely to be significant. Nevertheless, the results of future study (which includes some of the authors of this paper) could adjust the photometric zero points at the 0.03 mag level.

In this paper we continue to show all $F555W$ and $F814W$ magnitudes on the Holtzman et al. (1995b) system. Transformed magnitudes in V and I are shown with the 0.05 magnitude corrections, which is consistent with the final numbers shown in the previous papers of this series. The data can be updated for better corrections as they become available.

3.1.2. *Discovery and Classification of the Variable Stars*

The measured magnitudes and reported errors at all available epochs in *F555W* were used to identify variable stars using the method described by Saha & Hoessel (1990). The procedural details specific to the WFPC2 data in this series of papers has been given in Paper V, Saha et al. 1996b (Paper VI) and Saha et al. 1997 (Paper VIII). They are not repeated here.

All variable stars that were definitely so identified, are marked in Fig. 2. However some of the variables are not visible on these charts due to their extreme faintness combined with the variation in the background surface brightness on these images. The positions of these objects, as they appear in the images identified in the HST archives as *U5KY0201R* and *U2KY0202R* are listed in Table 2.

EDITOR: PLACE FIGURE 2 HERE.

EDITOR: PLACE TABLE 2 HERE.

The photometry on the Holtzman et al. (1995b) “short exposure” calibration system for the final list of 26 variable stars is presented in Table 3 for each epoch and each filter. The periods were determined with the Lafler-Kinman algorithm (1965) by using only the *F555W* passband data. Aliasing is not a serious problem for periods between 10 and 55 days because the observing strategy incorporated an optimum timing scheme as before in this series.

EDITOR: PLACE TABLE 3 HERE.

The resulting light curves in the $F555W$ passband, together with periods and mean magnitudes (determined by integrating the light curves, converted to intensities, and then converting the average back to magnitudes, and called the “phase-weighted intensity average” in Saha & Hoessel (1990)), are shown in Fig. 3, plotted in the order of descending period.

EDITOR: PLACE FIGURE 3 HERE.

All of the variable stars identified in this manner have periods and light curves consistent with being Cepheids. There is a range in the quality of the light curves – both in terms of the scatter in the individual points, as well as in the implied shapes. The object C3-V2, for instance, has an extremely small amplitude, even though its variability appears quite definite in signal-to-noise terms. It is possible that this is a blend of two stars, one of which may be a Cepheid. Thus sorting through the quality of each putative Cepheid is a necessary task, and is described later in this sub-section.

The available data for the variables in $F814W$ were folded with the ephemerides derived above using the $F555W$ data. The results are plotted in Fig. 4. All of the objects detected as variables in $F555W$ were recovered in at least 3 epochs in the $F814W$ observations.

The mean magnitudes in $F814W$ (integrated as intensities over the cycle) were obtained from the procedure of Labhardt, Sandage, & Tammann (1997) whereby each $F814W$ magnitude at a randomly sampled phase is converted to a mean value $\langle F814W \rangle$ using amplitude and phase information from the more complete $F555W$ light curves. Note that each available observation of $F814W$ is used independently to derive a mean magnitude. Hence, the scatter of the individual values about the adopted mean $F814W$ value is an *external* measure of the uncertainty in determining $\langle F814W \rangle$. It is this external measure of the uncertainty that is retained and propagated in the later calculations.

EDITOR: PLACE FIGURE 4 HERE.

The prescription given in Paper V for assigning the light-curve quality index QI (that ranges from 0 to 6) was used. In this scheme, a grade (0 – 2) is given for the quality of the $F555W$ light curves, with additional points (0 – 2) for the evenness in phase coverage of the five (or fewer) $F814W$ observation epochs, and up to three additional points (1 – 3) for the amplitude and phase coherence of the $F814W$ observations compared with the $F555W$ light curve. Hence, a quality index of 6 indicates the best possible light curve set in both $F555W$ and $F814W$. A quality index of 2 or less indicates near fatal flaws such as apparent phase incoherence in the two passbands. This is generally the indication that object confusion by crowding and/or contamination by background is likely. The weighting scheme puts a lot of weight on how well matched the few $F814W$ observations are to the light curve implied by the $F555W$ data. This is by design, since if reddening effects are to be deciphered from the Cepheid colors, the fidelity of the colors must be established, since color uncertainties dominate the error in the de-reddened distance modulus.

Table 4 lists the characteristics of all 26 putative Cepheids mentioned above. The $F555W$ and $F814W$ instrumental magnitudes of Table 3 have been converted to the Johnson V and Cousins (Cape) I standard photometric system by the color equations used in previous papers of this series, as set out in equations (2) and (3) of Paper V, based on the transformations of Holtzman et al. (1995b). In addition, as discussed in the previous sub-section, a value of 0.05 mag has been added to each of the V and I magnitudes to correct the Holtzman et al. (1995b) scales for the charge-transfer inefficiency problems. This correction is consistent with that used in all previous papers of this series, except that in the previous papers, the correction was applied at the end, to the distance moduli, and not in the tables corresponding to Table 4 here.

EDITOR: PLACE TABLE 4 HERE.

3.2. HSTphot based photometry

A parallel photometry procedure was carried through by one of us (AED) using the HSTphot stellar photometry package Dolphin (2000a). The images were masked using the data quality images, and pairs of images combined for cosmic ray removal using HSTphot’s *crclean* algorithm, producing eleven F555W and five F814W images (all 5000s) at the primary pointing, and a twelfth F555W image (also 5000s) at the secondary pointing.

The *multiphot* algorithm was used to simultaneously photometer all sixteen images at the primary pointing. Because of the distance to NGC 3982, it was extremely difficult to locate individual stars for use as PSF stars. Instead, the photometry was run twice: the first time using a library PSF calculated from Tiny Tim (Krist 1995) models, and the second time adding a residual (calculated from the stars found in the first run) to the PSF.

This process was also completed on the single image at the secondary pointing. To arrive at our final HSTphot photometry, we used the Dolphin (2000b) formulae to make CTE corrections and calibrate to the standard *VI* system, and matched the secondary pointing photometry to the primary pointing, producing instrumental and standard magnitudes for each star at each epoch.

The post-photometry procedure to detect and characterize the Cepheids was essentially identical to that used with the DoPHOT photometry results. The main differences involved the minimum acceptable photometry quality used – the HSTphot analysis required that stars be found with $\chi < 2.0$ and $|\text{sharpness}| < 0.4$ in order to avoid blends and stars for which good photometry was impossible. We also required that a star have at least 10 such good photometry measurements to be considered in the analysis. The quality parameters

in the HSTphot-based analysis range from 0-4 (rather than 0-6), but are based on similar criteria – cleanness of both the F555W and F814W light curves, coherence between the light curves, and phase coverage.

Of the 26 variables found by DoPHOT, 13 were independently discovered from the HSTphot analysis. Ten of these 13 common Cepheids have HSTphot quality parameters of 3 or 4. The periods and mean V and I magnitudes derived from the HSTphot measurements alone for these 13 Cepheids are given in Table 5.

The results from the HSTphot based procedure are used to estimate the distance modulus in §4.3, and used as a sanity check for the results from DoPHOT.

EDITOR: PLACE TABLE 5 HERE.

4. The Period-Luminosity Relation and the Distance Modulus

4.1. The P-L Diagrams in V and I

As in the previous papers of this series we adopt the P-L relation in V from Madore & Freedman (1991) as

$$M_V = -2.76 \log P - 1.40 , \quad (1)$$

whose companion relation in I is

$$M_I = -3.06 \log P - 1.81 . \quad (2)$$

The zero point of equations (1) and (2) is based on an assumed LMC modulus of 18.50.

The P-L relations in V and I for the 26 Cepheids in Table 4 are shown in Fig. 5. The filled circles show objects with periods greater than 20 days that have a quality index of 3

or higher. The solid lines show the canonical slopes of the P-L relations in V and I with the vertical offset for apparent distance moduli $\mu_V = 32.00$ and $\mu_I = 31.90$ respectively. These values were chosen to be in visual conformity with the points shown as filled circles (they are not intended as a formal derivation of distance). The expected spread in each of the pass-bands due to the finite width of the instability strip (Sandage & Tammann 1968) is indicated by the flanking dashed lines. The observed scatter of the data outside these envelope lines is due to the combination of (1) measuring and systematic errors due to background and contamination, (2) the random error of photon statistics, (3) the large effects of the variable extinction evident from the dust lanes seen in the images, and (4) objects mis-identified as Cepheids.

EDITOR: PLACE FIGURE 5 HERE.

The variables with periods shorter than 20 days can be seen to fall systematically brighter. This is due to a bias at the faint end because Cepheids at short periods that are at the faint end of the intrinsic scatter about the mean P-L relation and fall below the detection limit in brightness do not populate the P-L relation. This adversely affects the fitting of the P-L relation. A cut off that rejects objects shorter than 20 days is a sensible precaution in this case, and such a period cut does not introduce a bias of its own.

4.2. Analysis of the P-L Relation

For a first estimate, using $A_V/A_I = 1.7$ (Scheffler 1982) along with the very preliminary apparent moduli in V and I of 32.00 and 31.90 respectively as estimated above yields a dereddened modulus $\mu_0 \approx 31.76$. To explore the presence of differential extinction and to treat the data accordingly, we use the tools developed in Paper V and further developed in subsequent papers of this series.

For each Cepheid we calculate the apparent distance moduli separately in V and in I from the P-L relations of equations (1) and (2) and the observed $\langle V \rangle$ and $\langle I \rangle$ magnitudes from Table 4. These apparent distance moduli, called U_V and U_I in columns (7) and (8) of Table 4, are calculated by

$$U_V = 2.76 \log P + 1.40 + \langle V \rangle , \quad (3)$$

and

$$U_I = 3.06 \log P + 1.81 + \langle I \rangle . \quad (4)$$

They are the same as equations (6) and (7) of Paper V.

If the differences between the V and I moduli are due solely to reddening, and if the dependence of the reddening curve on wavelength is the normal standard dependence as in the Galaxy, then the true modulus U_T is given by

$$U_T = U_V - R'_V \cdot (U_V - U_I) , \quad (5)$$

where R' is the ratio of total to selective absorption, $A_V/E(V - I)$. This is equation (8) of Paper V. However, equation (5) is valid only if the difference between U_V and U_I is due to extinction, not to correlated measuring errors.

The values of U_T are listed in column 9 of Table 4. These would be the true moduli, as corrected for normal extinction, assuming that there are no systematic measuring errors. The total rms uncertainty for each U_T value is listed in column 10. This uncertainty includes contributions from the estimated random measuring errors in the mean V and I magnitudes, (in columns 4 and 6), as propagated through the de-reddening procedure, as well as the uncertainty associated with the intrinsic width of the P-L relation (i.e. a given Cepheid may not be on the mean ridge-line of the P-L relation) as well as a ten percent uncertainty in the estimated period. The de-reddening procedure amplifies the measuring errors. Therefore many Cepheids are needed to beat down these large errors (notice some

very large values in column 10) in any final value of the modulus. The values shown in column 10 of Table 4 were calculated using equation (18) of Saha et al. 2000, and also correspond to σ_{tot} as defined in Paper V.

From the data in Table 4, the unweighted mean de-reddened modulus $\mu_0 = \langle U_T \rangle$ for all Cepheids with periods greater than 20 days with $QI \geq 3$ is 31.72 ± 0.14 mag, and the weighted (by $1/\sigma_{tot}^2$) value is also 31.72 ± 0.15 mag. The average (unweighted) *apparent* modulus μ_V for this sample of Cepheids is 31.99 ± 0.13 and the corresponding value for μ_I is 31.88 ± 0.12 . This implies $E(V - I) = 0.11 \pm 0.17$ and $A_V = 0.27 \pm 0.41$, where the symbols have their usual meaning.

We mention again that the derived U_T values are only meaningful under the assumption that the differences between U_V and U_I are due to reddening alone, in the absence of appreciable systematic and correlated measuring errors, or when the errors for $U_V - U_I$ are *distributed symmetrically*. If asymmetrical errors in V and I dominate over differential reddening, the U_T derived via equation (5) *will be systematically in error*.

A diagnostic diagram to test for the relative presence of bona-fide differential extinction versus scatter due to measuring errors alone was devised in Paper V, and used in subsequent papers of this series. We do not repeat its description. It is shown in Figure 6 for the Cepheids in NGC 3982. The filled circles again show Cepheids with periods greater than 20 days and with $QI \geq 3$. The solid line indicates the reddening vector for the P-L ridge line, if the true (de-reddened) distance modulus is 31.75 which is close to the initial estimate for the distance modulus made above. The dashed lines show the bounds due to the intrinsic dispersion of the P-L relation as explained in Paper V. The slope of the lines is $A_V/E(V - I) = 2.43$, in accordance with the reddening law of Scheffler (1982).

EDITOR: PLACE FIGURE 6 HERE.

The scatter in Fig. 6 does not lie within the reddening track. Translating the reddening band in this figure would not materially reduce the number of points that would spill out of it. There may be some differential reddening, but there is very significant scatter orthogonal to the reddening track, indicating that the range in U_V and U_I values is driven more by photometry errors rather than by extinction alone. As mentioned above, and discussed in previous papers of this series, any skewness in the distribution of measurement errors contributes to a systematic error in the de-reddened modulus for the galaxy.

4.2.1. *Distance Modulus from a Color-Selected Sample*

Since we have shown that the scatter in observed colors of the Cepheids is significantly due to observational errors, we can try to exclude color outliers by selecting out objects whose measured colors are extreme for Cepheids. To do this, we utilize the Period-Color (P-C) relation for Cepheids, which follows immediately from equations (1) and (2):

$$(V - I)_0 = 0.30 \log P + 0.41 \tag{6}$$

where $(V - I)_0$ is the intrinsic color of a Cepheid on the ridge line of the P-L relation. Note that the intrinsic scatter in color is small: the delimiting lines shown in Fig 5 map to lines 0.08 mag above and below the line defined above by eqn. (6). The ridge line summarized in Sandage, Bell, & Tripicco (1999) from independent data by Dean, Warren, & Cousins (1978), Caldwell & Coulson (1985) & Fernie (1990) is essentially identical to the above, as shown in Saha et al. 2001 (Paper X). The observed colors can be reddened by dust, and scatter will be introduced both, by differential extinction as well as measurement errors.

We expect to see some Cepheids that are reddened very little because they are on the near side of the disk. Others may have substantial reddening since they are seen through the disk, and possibly through dust lanes. The rationale for a color-cut is that while

bona-fide extinction should not affect the de-reddened distance modulus irrespective of how the data are cut in color, objects with large errors and objects mis-classified as Cepheids, which *do* affect the modulus, can be identified and rejected.

The P-C relation for the data at hand is shown in Fig 7. As before, the filled circles indicate Cepheids with $P \geq 20$ and $QI \geq 3$.

A plot of individual de-reddened moduli U_T vs. color deviation $\Delta(V - I) = U_V - U_I$ from the fiducial PC relation for the data at hand is shown in Fig 8, again where filled circles indicate Cepheids with $P \geq 20$ and $QI \geq 3$. This diagram graphically demonstrates that the derived distance is a strong function of the measured color, showing again that the data are dominated by measurement errors. An inspection of this figure indicates that values of $U_V - U_I$ less than -0.2 or greater than 0.4 are almost certainly outliers: rejecting these and working with the 14 Cepheids with $P \geq 20$ and $QI \geq 3$ yields a de-reddened modulus $\mu_0 = 31.71 \pm 0.14$. This cut corresponds to a region delimited by a line 0.2 mag below and a line 0.4 mag above the ridge line of the fiducial PC relation shown in Fig 7.

A way to arrive at a less arbitrary cut is to try various cuts by color, and choose the one(s) that produce the P-L relations with the least scatter in both passbands. Following such a path, we arrive at a cut with $-0.2 \leq U_V - U_I \leq 0.3$, which corresponds to a line 0.2 mag below and a line 0.3 mag above the ridge line of the fiducial PC relation. This cut yields $\mu_0 = 31.82 \pm 0.14$, using the 12 acceptable Cepheids that also have $P \geq 20$ and $QI \geq 3$.

4.3. Distance Estimate from the HSTphot results

We consider here the sample of Cepheids found using the HSTphot photometry, as described in §3.2. Recall that 13 Cepheids were reported, all in common with the DoPHOT

based discoveries. A different grading scheme with grades from 0-4 was used, and assigned independently. Using the 10 Cepheids which have $P \geq 20^d$ and grade 3 or better, and computing the de-reddened moduli U_T we find that C1-V2 is a clear outlier (too large a modulus). Using the remaining 9 Cepheids, we arrive at a mean (unweighted) de-reddened distance modulus $\mu_0 = 31.85 \pm 0.16$. This is within the errors of the similar calculation for DoPHOT based Cepheids. This subsample of 9 Cepheids with HSTphot photometry gives $\mu_V = 32.26 \pm 0.08$ and $\mu_I = 32.09 \pm 0.09$, implying $E(V - I) = 0.17 \pm 0.12$ and $A_V = 0.41 \pm 0.29$.

4.4. The Adopted Distance Modulus

We are satisfied that the results from HSTphot are consistent within the errors with the DoPHOT results, and having used this as a sanity check, proceed with the DoPHOT values.

The various cuts on the DoPHOT sample of Cepheids were discussed in §4.2. The results do not change significantly within the errors irrespective of the subsample used. We therefore adopt the most robust cut of all, which is the one with $P \geq 20^d$ and $QI \geq 3$, which was shown to yield:

$$\mu_0 = 31.72 \pm 0.14 \tag{7}$$

and

$$E(V - I) = 0.11 \pm 0.17 \tag{8}$$

The apparent distance modulus in the V band is given by

$$\mu_V = 31.99 \pm 0.13 \tag{9}$$

Looking back over the Cepheid measurements made in this series of papers, we note that the photometry has been most troublesome in the those galaxies where the disk is inclined to the line of sight. The 2 farthest galaxies of this study, NGC 4639 and NGC 3982, presented no photometric inconsistencies. Both these galaxies present face-on disks. By contrast, it was necessary to examine the data most critically for NGC 4527 and NGC 3627, which are both closer in distance modulus by at least a magnitude. However their disks are very inclined, thus presenting a higher column density of stars which may be contributing more severely to contamination and confusion noise.

5. The Type Ia Supernova 1998aq

SN 1998aq was discovered in NGC 3982 by M. Armstrong (Hurst et al. 1998). Pre-maximum and subsequent spectroscopy revealed it to be a prototype SNIa (Ayani & Yamaoka 1998; Berlind & Calkins as quoted by Garnavich et al. 1998; Vinkó et al. 1999). The SN reached B -maximum on JD 2 450 931 and had a normal decline rate of $\Delta m_{15} = 1.12 \pm 0.05$ (Riess et al. 1999).

The light curve of SN 1998aq, as compiled from amateur observations by the *Variable Star Observers' Network* (VSNET), indicates an apparent maximum V -magnitude of $m_V(\text{max}) = 12.30 (\pm 0.15)$. CCD-photometry six days before B -maximum showed that the SN had $m_V = 12.67 (\pm 0.05)$ (Hanzl & Caton 1998). At this epoch a SNIa is $0.40 (\pm 0.05)$ below V -maximum (Leibundgut 1995 - private communication; Riess et al. 1999). From this follows $m_V(\text{max}) = 12.27 (\pm 0.10)$ in fortuitous agreement with the above value. We will adopt $m_V(\text{max}) = 12.28 \pm 0.08$.

On the assumption that SN 1998aq suffers the same reddening of $E(B - V) = 0.09$ (of which 0.01 is due to Galactic reddening; Schlegel, Finkbeiner, & Davis 1998) as an average

Cepheid in NGC 3982, the absolute magnitude of the SN is obtained by simply subtracting the *apparent* V -modulus of $\mu_V = 31.99 \pm 0.13$ from the *apparent* maximum V -magnitude of the SN of $m_V(\text{max}) = 12.28 \pm 0.08$. This gives

$$M_V(\text{max}) = -19.71 \pm 0.15 \quad (10)$$

for SN 1998aq. This value is brighter than that of any of the eight Cepheid-calibrated normal SNe Ia (Parodi et al. 2000, Tammann, Sandage, & Saha 2001), but not significantly so. It is therefore unlikely that we have underestimated the absorption of the SN. If the absolute magnitude is reduced to the standard decline rate of $\Delta m_{15} = 1.2$ by means of equation (10) by Parodi et al. (2000) one obtains

$$M_V^{\text{corr}} = -19.67 \pm 0.15. \quad (11)$$

Of course, it is possible that SN 1998aq suffers only the Galactic reddening of $E(B - V) = 0.014$ and very little or no additional reddening in its parent galaxy. The absence of NaD absorption lines in its spectrum (Ayani & Yamaoka 1998) may be taken as a hint in this direction. If the SN indeed suffered no absorption in NGC 3982, its absolute magnitude would become fainter by $3.1 \times 0.076 = 0.24$ mag than quoted above, i.e.

$$M_V(\text{max}) = -19.47 \pm 0.15 \quad (12)$$

$$M_V^{\text{corr}} = -19.43 \pm 0.15. \quad (13)$$

This is a firm lower limit to the luminosity of SN 1998aq because it cannot suffer less than zero absorption. Yet it is only insignificantly fainter than the *mean* of the eight Cepheid-calibrated SNe Ia of $\langle M_V^{\text{corr}} \rangle = -19.48 \pm 0.07$ (Parodi et al. 2000).

Carrying the discussion one step further, it is noted that SN 1998aq is quoted by an anonymous referee to the paper by Vinkó et al. (1999) as having had $(B - V) = -0.17$ six days before B -maximum. With $m_V = 12.67$ from above for the same epoch and

considering that a SNIa is then 0.28 mag below B -maximum (Leibundgut 1995 – private communication; Riess et al. 1999), one obtains $m_B(\text{max}) = 12.22 (\pm 0.10)$. From this follows $(B - V) = -0.06 (\pm 0.14)$, i.e. a value which happens to agree very well with the mean intrinsic color of normal SNe Ia with $\langle B - V \rangle = -0.013$, $\sigma = 0.06$ (Parodi et al. 2000). It seems therefore that SN 1998aq indeed suffers very little absorption in its parent galaxy.

It should be mentioned that there is another color measurement of SN 1998aq six days before B -maximum giving $(B - V) = +0.02$ (Hanzl & Caton 1998). This very red pre-maximum color would imply a reddening of $E(B - V) \approx 0.2$. The corresponding absorption of $A_B \approx 0.8$ and $A_V \approx 0.6$ would give to SN 1998aq an absolute magnitude around $M_B(\text{max}) \approx M_V(\text{max}) \approx -20.0$. The only SNIa known to have become so luminous is SN 1995ac (Saha et al. 2001) which, however, had a peculiar SN 1991T-like spectrum and which is definitely not shared by SN 1998aq. We conclude therefore that the published color of $(B - V) = +0.2$ must be erroneous.

If the adopted values of $m_B(\text{max}) = 12.22$ and $m_V(\text{max}) = 12.28$ are corrected for Galactic reddening of $E(B - V) = 0.014$ one obtains $m_B^0(\text{max}) = 12.16 (\pm 0.15)$ and $m_V^0(\text{max}) = 12.24 (\pm 0.14)$. With a true modulus of NGC 3982 of $(m - M)^0 = 31.72 \pm 0.14$ the absolute magnitudes become then

$$M_B^0(\text{max}) = -19.56 \pm 0.21, \quad M_V^0(\text{max}) = -19.48 \pm 0.20. \quad (14)$$

These values can now be reduced to the standard values of $\Delta m_{15} = 1.2$ and $(B - V) = -0.01$ using equations (9) and (10) of Parodi et al. (2000) giving

$$M_B^{\text{corr}} = -19.35 \pm 0.24, \quad M_V^{\text{corr}} = -19.34 \pm 0.23. \quad (15)$$

The value of M_V^{corr} found here compares well with that in equation (13).

6. The value of H_0

There are now nine SNeIa with Branch-normal spectra whose Cepheid distances are known. They are compiled in Table 6. The reader can find the input data and the original sources in Parodi et al. (2000).

EDITOR: PLACE TABLE 6 HERE.

SN 1895B is omitted because its V -magnitude at maximum is unreliable. We have also determined a Cepheid distance for SN 1991T (Saha et al. 2001), but this object should not be used as a calibrator in view of its peculiar spectrum and its poorly known internal absorption (cf. however Gibson & Stetson 2000; Gibson & Brook 2000). The yet incomplete data on SN 1991T-like SNe suggest that they form a quite heterogeneous class (Saha et al. 2001).

The absolute magnitudes of the nine calibrating SNeIa in columns (9) – (11) of Table 6 are corrected for decline rate Δm_{15} and variations of the intrinsic color ($B_{\max} - V_{\max}$). They are reduced to a standard SNIa with $\Delta m_{15} = 1.2$ and $(B_{\max} - V_{\max}) = -0.01$. The relevant reduction formulae are given by Parodi et al. (2000; eq. 9 – 11; for quite similar reduction formulae cf. Tripp 1998, and Tripp & Branch 1999).

The value of H_0 is obtained by fitting the weighted $\langle M_{\lambda}^{\text{corr}} \rangle$ of the calibrators to a sample of more distant, absorption-free Branch-normal SNeIa. We use here the fiducial sample of the 35 bluest SNeIa as defined by Parodi et al. (2000). They suffer minimum internal absorption, and their mean color of $(B_{\max} - V_{\max}) = -0.012 \pm 0.008$ perfectly matches the mean color of the calibrators of -0.017 ± 0.015 . The agreement in color, which is not affected by the corrections for Δm_{15} and intrinsic variations of $(B_{\max} - V_{\max})$, is decisive for the determination of H_0 . It does not necessarily mean that we have found the

true intrinsic color of SNe Ia, but it shows that any remaining absorption is the same for the calibrators and for the fiducial sample, and this is a sufficient condition for the derivation of reliable distances.

The 35 SNe Ia of the fiducial sample have a velocity restriction of $1200 < v \lesssim 30\,000 \text{ km s}^{-1}$. The lower limit is set to reduce the effect of peculiar velocities, the upper limit to keep space curvature effects small, but still to reflect the *large-scale* value of H_0 . Fitting a straight line to the fiducial sample of the form

$$\log v = 0.2 m_\lambda + c_\lambda \quad (16)$$

is indistinguishable from the case of a flat Universe with $\Omega_M = 1$. A presently favored model with $\Omega_M = 0.3, \Omega_\Lambda = 0.7$ yields a value of H_0 which is only 0.8 units higher (cf. Parodi et al. 2000). We pursue the $\Omega_M = 1$ case for the sake of simplicity and comparison with external results.

A trivial transformation of equation (16) leads to

$$\log H_0 = 0.2 M_\lambda + 5 + c_\lambda. \quad (17)$$

The constant c_λ is defined by the fiducial sample to be $c_B = 0.676 \pm 0.004$, $c_V = 0.673 \pm 0.004$, and $c_I = 0.616 \pm 0.004$. Inserting these values together with the appropriate values of $\langle M_\lambda^{\text{corr}} \rangle$ from Table 6 into equation (17) yields $H_0(B) = 60.5 \pm 2.0$, $H_0(V) = 60.4 \pm 1.8$, and $H_0(I) = 60.0 \pm 2.8$, i.e. almost identical values in the three wave bands. We adopt at this point $H_0 = 60.3 \pm 1.8$ for the case $\Omega_M = 1$.

Gibson et al. (2000) have re-analyzed the *HST* Cepheid observations of Saha et al. (1994, 1995, 1996a,b, 1997, 1999) and Tanvir et al. (1995) and have obtained distances which are smaller by 0^m14 on average than the moduli shown in Table 6. The largest deviation of 0^m49 is suggested for NGC 5253; however, the corresponding small modulus of $(m - M)^0 = 27.61$ would imply an exceptionally faint tip of the red-giant branch of

NGC 5253 (Saha et al. 1995) as well as of NGC 5128, another member of the Cen A group. Also the surface brightness fluctuation method, albeit with its attendant uncertainties, gives $(m - M)^0 = 28.13$ for NGC 5128 and for NGC 5102, which both belong to the same group (Ferrarese et al. 2000). If NGC 5253 is excluded, the Gibson et al. moduli are still systematically smaller by $0^m11 \pm 0.03$ than adopted in Table 6 for the first seven entries. We stand by our original numbers, and emphasize that the 118 Cepheids *in common* between the work of Gibson et al. and Saha et al. agree within a few 0^m01 (Gibson et al. 2000, Table 3; Parodi et al. 2000). The differences in distances derived by these 2 sets of reductions must therefore lie in the different samples of Cepheids chosen. It is easily demonstrated, say for the specific case of NGC 5253, that the sample of common Cepheids with Gibson et al.’s photometry yields a distance that is significantly higher than what is obtained using all of their Cepheids. This is an important point for other reasons as well: the distances to all galaxies studied by the Mould, Freedman, Kennicutt et al. (MFK) consortium *except* for the ones that are a re-analysis of the SNe Ia bearing galaxies first studied by the Sandage et al. consortium, are based on a Cepheids found in *common* by the DAOPHOT and DoPHOT based procedures. For this reason, the Gibson et al. (2000) re-analysis is not at par with the distances for other galaxies studied by the MFK consortium. If the Cepheids that are found in common by Gibson et al. (2000) and by us (in the previous papers in this series) are used, even with just the Gibson et al. photometry, the resulting distances to the galaxies are in general larger than the ones reported by Gibson et al. (2000), by amounts that vary from one galaxy to another, with NGC 5253 being the most striking case. Despite these considerations, if the smaller Cepheid distances of Gibson et al. (2000) are taken at face value, excluding only NGC 5253, the value of $H_0 = 60.3$ above is increased to $H_0 = 63.4$. If these authors had applied the metallicity corrections of Cepheid distances as now adopted by Freedman et al. (2001), they would have obtained $H_0 = 61.7$, a value quite close to ours, but for different reasons.

Freedman et al. (2001) have decreased the Gibson et. al. distances of the first eight galaxies in Table 6 by an additional 0^m09 on average. The proposed increase is the net result of two effects. (1) The authors adopt a metallicity dependence of the Cepheid distances, which *increases* their distances by 0^m06 on average. (2) They use the Cepheid PL relation in V and I as derived by Udalski et al. (1999) from OGLE survey data. The unexpectedly flat slope of their I -band PL relation increases the absorption corrections of the long-period Cepheids and results in a *decrease* of the Gibson et al. distances by 0^m15 . The new I -band relation needs further confirmation. The new PL relations imply a very flat color-period relation of

$$(V - I) = 0.202 \log P + \text{const} , \quad (18)$$

which disagrees with the results discussed by Sandage, Bell & Tripicco (1999) that are based on the extensive color data of Dean, Warren & Cousins (1978) and Caldwell & Coulson (1984, 1985). The color-period relation implied by the multi-color PL relations from Madore & Freedman (1991), as well as from Feast & Walker (1987) are in agreement with the results discussed by Sandage, Bell & Tripicco (1999), but they all disagree with the results of Udalski et al. (1999), whose sample does not include variables with $\log P > 1.5$ because, as stated in their paper, they are too bright and are saturated in the OGLE images. Yet such longer-period Cepheids are effectively the ones to which the Freedman et al. (2001) correction applies.

If we adopt for the moment the new distances of Freedman et al. (2001; Table 4) for the first eight galaxies in Table 6 – which reduces the adopted moduli by 0^m25 on average – we find $H_0 = 67.7$ instead of $H_0 = 60.3$ from above.

There remains the question why we obtain $H_0 = 67.7$ even if we adopt the Freedman et al. (2001) distances at face value, while these authors suggest $H_0 = 71$ from SNeIa alone. There are mainly three rather subtle reasons. (1) Freedman et al. use only six

SNeIa as calibrators. Their questionable distance for SN 1972E in NGC 5253 therefore contributes with higher weight. If this object is excluded, their H_0 decreases by 2.5 percent. (2) There is a slight color mismatch between the calibrators and the distant sample as used by Freedman et al. After application of their absorption and decline rate corrections, their six calibrators have a mean color of $(B - V)^{\text{corr}} = -0.043 \pm 0.008$, while the mean color of their distant SNeIa sample is $(B - V)^{\text{corr}} = -0.061 \pm 0.002$, i.e. they are very blue. Obviously the distant sample is overcorrected for internal absorption. The difference $\Delta E(B - V) = 0.018 \pm 0.008$ translates into a reduction of the moduli of the distant SNeIa by $\Delta m_B = 0.074$, $\Delta m_V = 0.056$, and $\Delta m_I = 0.033$. If we correct for this mis-match in color, their value for H_0 is reduced by another 2.6 percent. (3) The calibrating SNeIa lie in spirals and hence have slower decline rates than the distant SNeIa which come in all types of galaxies. In the case of Freedman et al. (2001) the mean difference amounts to $\delta \Delta m_{15} = 0.20$. This value must be multiplied by the wavelength-dependent slope of the Δm_{15} -luminosity relation to allow a fair comparison between calibrators and distant SNeIa. The authors have adopted the rather steep slope of Hamuy et al. (1996), yet an enlarged sample of SNeIa gives a significantly smaller slope (Parodi et al. 2000; equations 3-5). The calibrating SNeIa have therefore been overcorrected faintwards by $0^{\text{m}}06$, $0^{\text{m}}04$, and $0^{\text{m}}04$ in B , V , and I , respectively. This has led to an overestimate of H_0 by ~ 2 percent. – If these three points are allowed for, the value of $H_0 = 71$ by Freedman et al. (2001) comes very close to the value of $H_0 = 67.7$, which we have derived above using their new Cepheid distances.

Pending a re-reduction of all *HST* Cepheid observations entering Table 6 we leave it to the reader to weight our Cepheid distances, those by Gibson et al. (2000), as well as the ones by Freedman et al. (2001) based on Udalski et al.’s (1999) yet unconfirmed PL relation. At present we adopt the distances in Table 6 and hence $H_0 = 60.3 \pm 1.8 (\Omega_M = 1)$ or $H_0 = 61.1 \pm 1.8 (\Omega_M = 0.3, \Omega_\Lambda = 0.7)$.

It should be noticed that remaining systematic error sources tend to reduce the true value of H_0 . In particular there is increasing evidence that the zero point of the PL relation with LMC at $(m - M)^0 = 18.50$ should be made brighter by $\sim 0^m06$ (cf. Tammann, Sandage, & Saha 2001). Moreover, if we would apply the metallicity corrections of the Cepheid distances adopted by Freedman et al. (2001) the distances would increase by an additional 0^m06 . Summarizing the systematic error sources Parodi et al. (2000) have conservatively estimated the correction factor of H_0 to be 0.96 ± 0.08 . This leads to

$$H_0 = 58.7 \pm 6.3, \tag{19}$$

including systematic errors and valid for a model with $\Omega_M = 0.3, \Omega_\Lambda = 0.7$.

We thank the many individuals at STScI who have worked hard behind the scenes to make these observations possible. Support for this work was provided by NASA through grant # HST-GO-08100.01A from the Space Telescope Science Institute, which is operated by the Association of Universities for Research in Astronomy, Inc., under NASA contract NAS5-26555. G.A.T. thanks the Swiss National Science Foundation for continued support.

REFERENCES

- Ayani, K., & Yamaoka, H. 1998, IAU Circ. 6878, 2
- Branch, D. 2001, PASP, 113, 169
- Branch, D., Fisher A., & Nugent, P. 1993, AJ, 106, 2383
- Caldwell, J.A.R., & Coulson, I.M. 1984, SAAO Circ. 8, 1
- Caldwell, J.A.R., & Coulson, I.M. 1985, MNRAS, 212, 879
- Dean, J.F., Warren, P.R., & Cousins, A.W.J. 1978, MNRAS, 183, 569
- de Vaucouleurs, G. 1975 in Galaxies and the Universe, eds. A. Sandage, M. Sandage, & J. Kristian, Vol 9 of Stars and Stellar Systems (Chicago: University of Chicago Press), Chapter 14, p 557
- Dolphin, A.E. 2000a, PASP, 112, 1383
- Dolphin, A.E. 2000b, PASP, 112, 1397
- Feast, M.W. & Walker, A.R. 1987, ARA&A, 25, 345
- Ferrarse, L., et al. 2000, ApJ, 529, 745
- Fernie, J.D. 1990, ApJ, 354, 295
- Freedman, W.L., et al. 2001, ApJ, astro-ph/0012376
- Garnavich, P., et al. 1998, IAU Circ. 6880, 2
- Gibson, B.K., & Brook, C.B. 2000, astro-ph/0011567
- Gibson, B.K., & Stetson, P.B. 2000, ApJ, 547, 103

- Gibson, B.K., et al. 2000, ApJ, 529, 723
- Hamuy, M., Phillips, M.M., Schommer, R.A., Suntzeff, N.B., Maza, J., & Aviles, R. 1996a, AJ, 112, 2398
- Hamuy, M., Phillips, M.M., Suntzeff, N.B., Schommer, R.A., Maza, J., Smith, R.C., Lira, P., & Aviles, R. 1996b, AJ112, 2438
- Hanzl, D., & Caton, D.B. 1998, IAU Circ. 6898, 5
- Holtzman, J.A., et al. 1995a, PASP, 107, 156
- Holtzman, J.A., et al. 1995b, PASP, 107, 1065
- Humason, M.L., Mayall, N.U. & Sandage, A. 1956, AJ, 61, 97
- Hurst, G.M., Armstrong, M., & Arbour, R. 1998, IAU Circ. 6875, 1
- Krist, J. 1995, ADASS IV, 349
- Labhardt, L., Sandage, A., & Tammann, G.A. 1997, A&A, 322, 751
- Lafler, J. & Kinman, T.D. 1965, ApJS, 11, 216
- Leibundgut, B. 1995, private communication
- Madore, B.F., & Freedman, W.L. 1991, PASP, 103, 933
- Madore, B.F. et al. 1999, ApJ, 515, 29
- Nolthenius, R. 1993, ApJS, 85, 1
- Parodi, B.R., Saha, A., Sandage, A., & Tammann, G.A. 2000, ApJ, 540, 634
- Phillips, M.M., Lira, P., Suntzeff, N.B., Schommer, R.A., Hamuy, M., & Maza, J. 1999, AJ, 118, 1766

- Pierce, M.J. & Tully, R.B. 1988, ApJ, 330, 579
- Riess, A.G., et al. 1999, AJ, 118, 2675
- Saha, A., & Hoessel, J.G. 1990, AJ, 99, 97
- Saha, A., Labhardt, L., Schwengeler, H., Macchetto, F.D., Panagia, N., Sandage, A., & Tammann, G.A. 1994, ApJ, 425, 14
- Saha, A., Sandage, A., Labhardt, L., Schwengeler, H., Tammann, G.A., Panagia, N., & Macchetto, F.D. 1995, ApJ, 438, 8
- Saha, A., Sandage, A., Labhardt, L., Tammann, G.A., Macchetto, F.D., & Panagia, N. 1996a, ApJ, 466, 55 (Paper V; NGC 4536; SN 1981B)
- Saha, A., Sandage, A., Labhardt, L., Tammann, G.A., Macchetto, F.D., & Panagia, N. 1996b, ApJS, 107, 693 (Paper VI; NGC 4496A; SN 1960F)
- Saha, A., Sandage, A., Labhardt, L., Tammann, G.A., Macchetto, F.D., & Panagia, N. 1997, ApJ, 486, 1 (Paper VIII; NGC 4639; SN 1990N)
- Saha, A., Sandage, A., Tammann, G.A., Labhardt, L., Macchetto, F.D., & Panagia, N. 1999, ApJ, 522, 802 (Paper IX; NGC 3627; SN 1989B)
- Saha, A., Labhardt, L., Prosser, C. 2000, PASP, 112, 163.
- Saha, A., et al. 2001, ApJ, 551, 973 (Paper X; NGC 4527; SN 1991T)
- Sandage, A., Bell, R.A., & Tripicco, M.J. 1999, ApJ, 522, 250
- Sandage, A., & Tammann, G.A. 1968, ApJ, 151, 531
- Sandage, A., & Tammann, G.A. 1982, ApJ, 256, 339 (Steps VII)

- Sandage, A., & Tammann, G.A. 1987, *A Revised Shapley-Ames Catalog of Bright Galaxies*, 2nd ed., (Washington: Carnegie Institution)
- Schechter, P.L., Mateo, M.L., & Saha, A. 1993, *PASP*, 105, 1342
- Scheffler, H. 1982, in *Landolt-Börnstein, Astronomy & Astrophysics*, vol. 2c, eds. K. Schaifers & H.H. Voigt (Berlin: Springer), p46
- Schlegel, D.J., Finkbeiner, D.P., & Davis, M. 1998, *ApJ*, 500, 525
- Stanek, K.Z. & Udalski, A. 1999, *astro-ph/99 09 346*
- Tammann, G.A., Sandage, A., & Saha, A. 2001, in: *A Decade of HST Science*, eds. M. Livio, K. Noll, & M. Stiavelli, (Cambridge: Cambridge University Press), in press, *astro-ph/00 10 422*
- Tanvir, N.R., Shanks, T., Ferguson, H.C., & Robinson, D.T.R. 1995, *Nature*, 377, 27
- Tripp, R. 1998, *A&A*, 331, 815
- Tripp, R., & Branch, D. 1999, *ApJ*, 525, 209
- Tully, R.B. 1988, *Nearby Galaxy Catalog* (Cambridge: Cambridge University Press).
- Tully, R.B. & Fisher, J.R. 1987, *Atlas of Nearby Galaxies* (Cambridge: CUP), Map 15
- Tully, R.B., Verheijen, M.A.W., Pierce, M.J., Huang, J-S, & Wainscoat, R.J. 1996, *AJ*, 112, 2471
- Udalski, A. et al. 1999, *Acta Astron.* 49, 201
- Verheijen, M.A.W. 1987, PhD thesis, University of Groningen
- Vinkó, J., Kiss, L.L., Thomson, J., Furész, G., Lu, W., Kaszás, G., & Balog, Z. 1999, *A&A*, 345, 592 R. 1985, *ApJ*, 313, L69

Whitmore, B., Heyer, I., & Casertano, S. 1999, 111, 1559

Fig. 1.— Mosaic V image of NGC 3982 showing the field imaged with the WFPC2. The orientation on the sky is also indicated.

Fig. 2.— Identifications for all the variable stars found. The numbers are the same as in Tables 2 to 5. Each of the four WFPC2 chips is shown separately. The orientation on the sky is indicated on each of the panels.

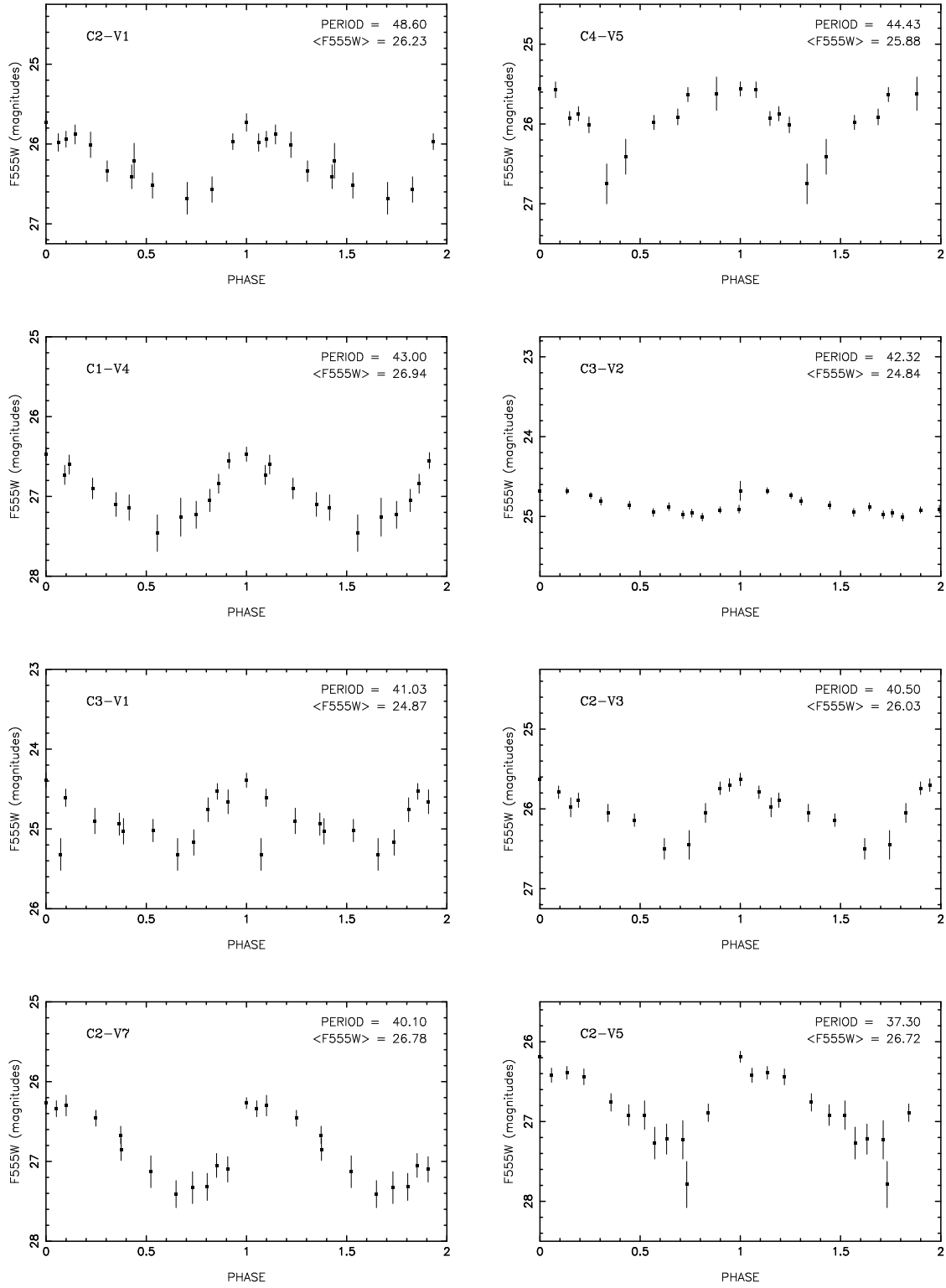
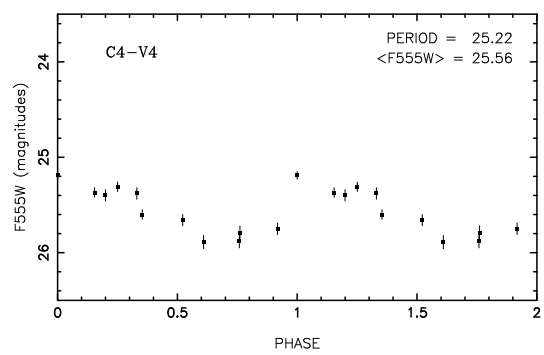
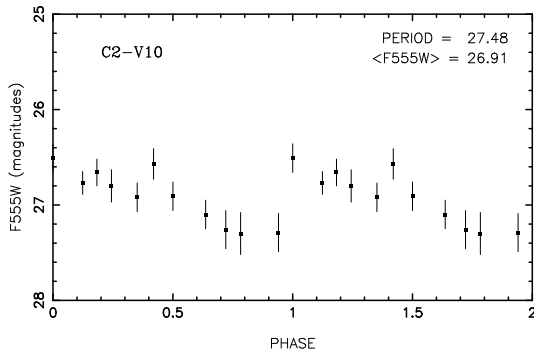
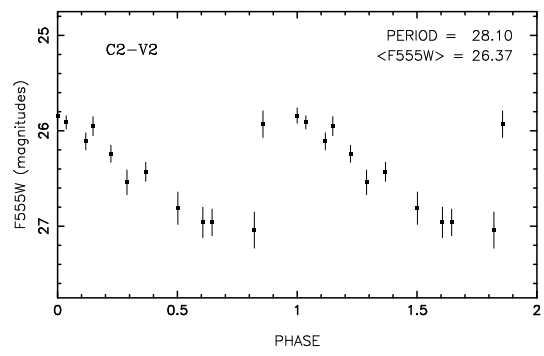
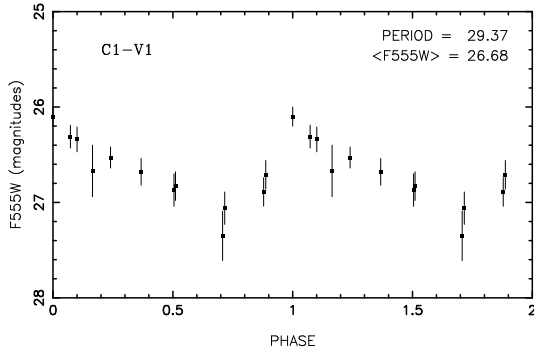
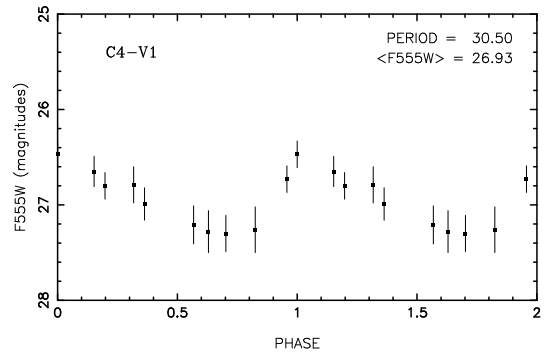
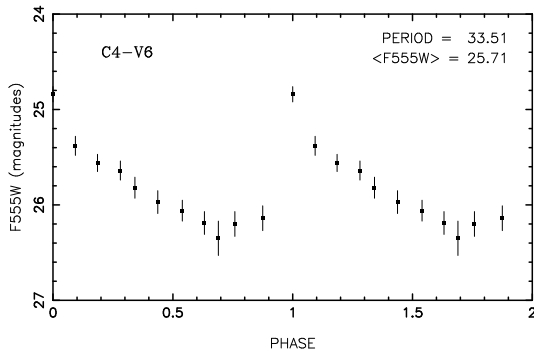
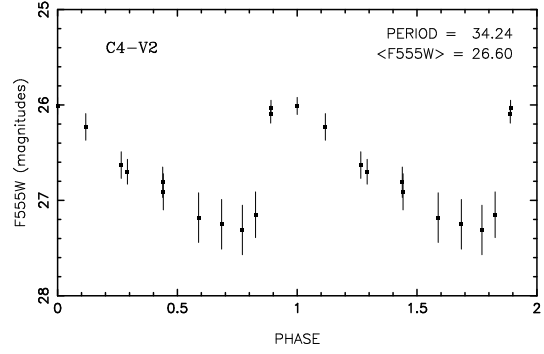
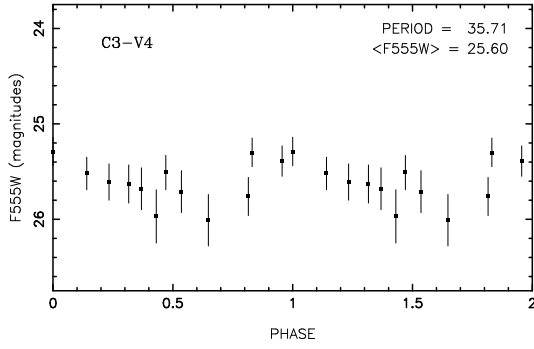
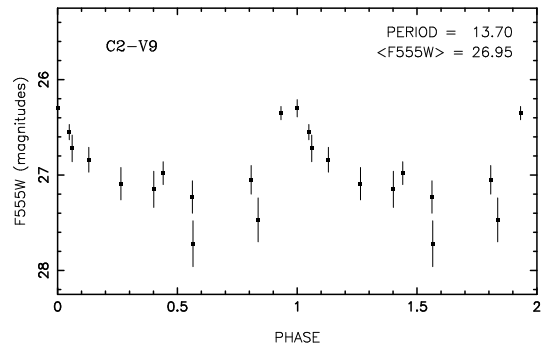
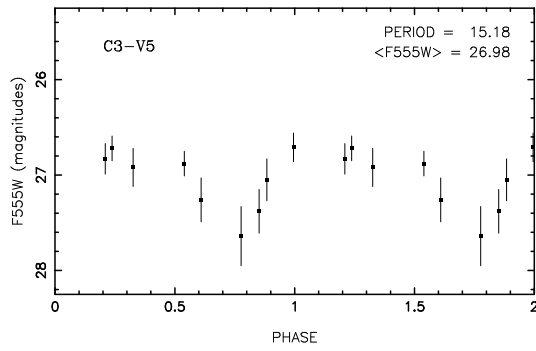
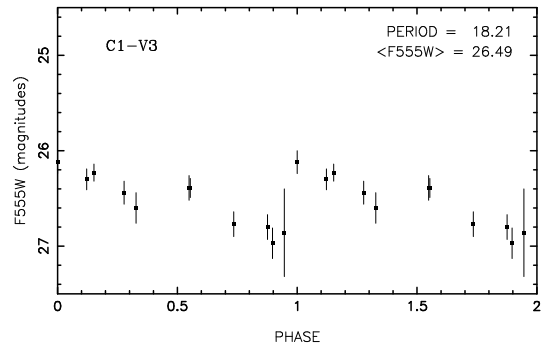
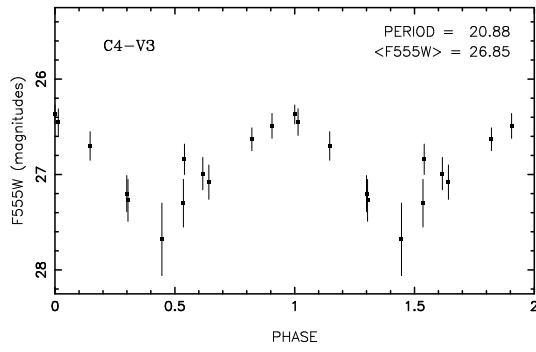
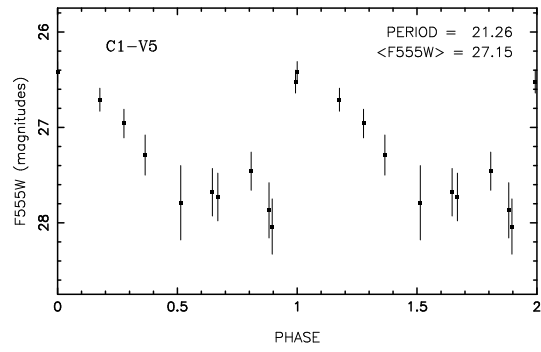
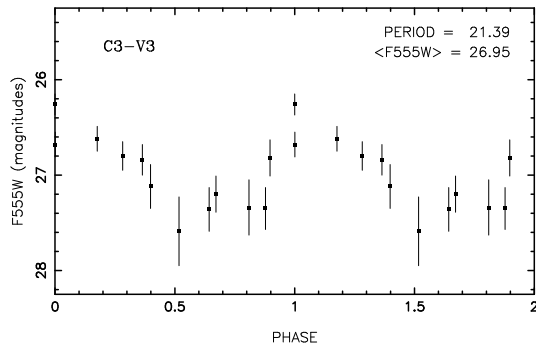
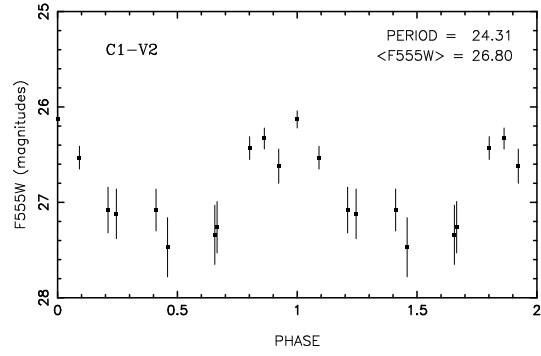
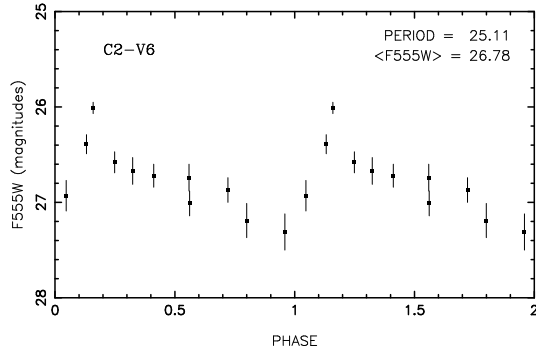
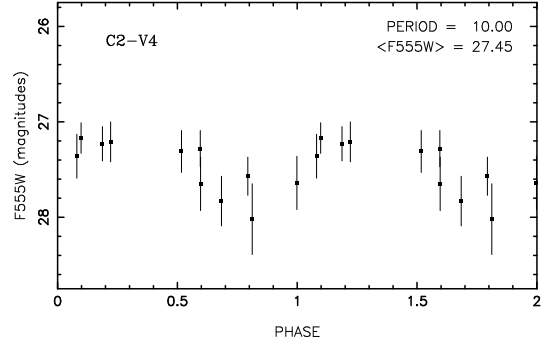
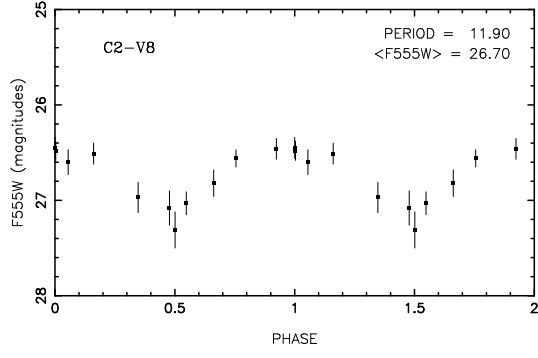


Fig. 3.— Light curves, plotted in order of period, in the $F555W$ band.







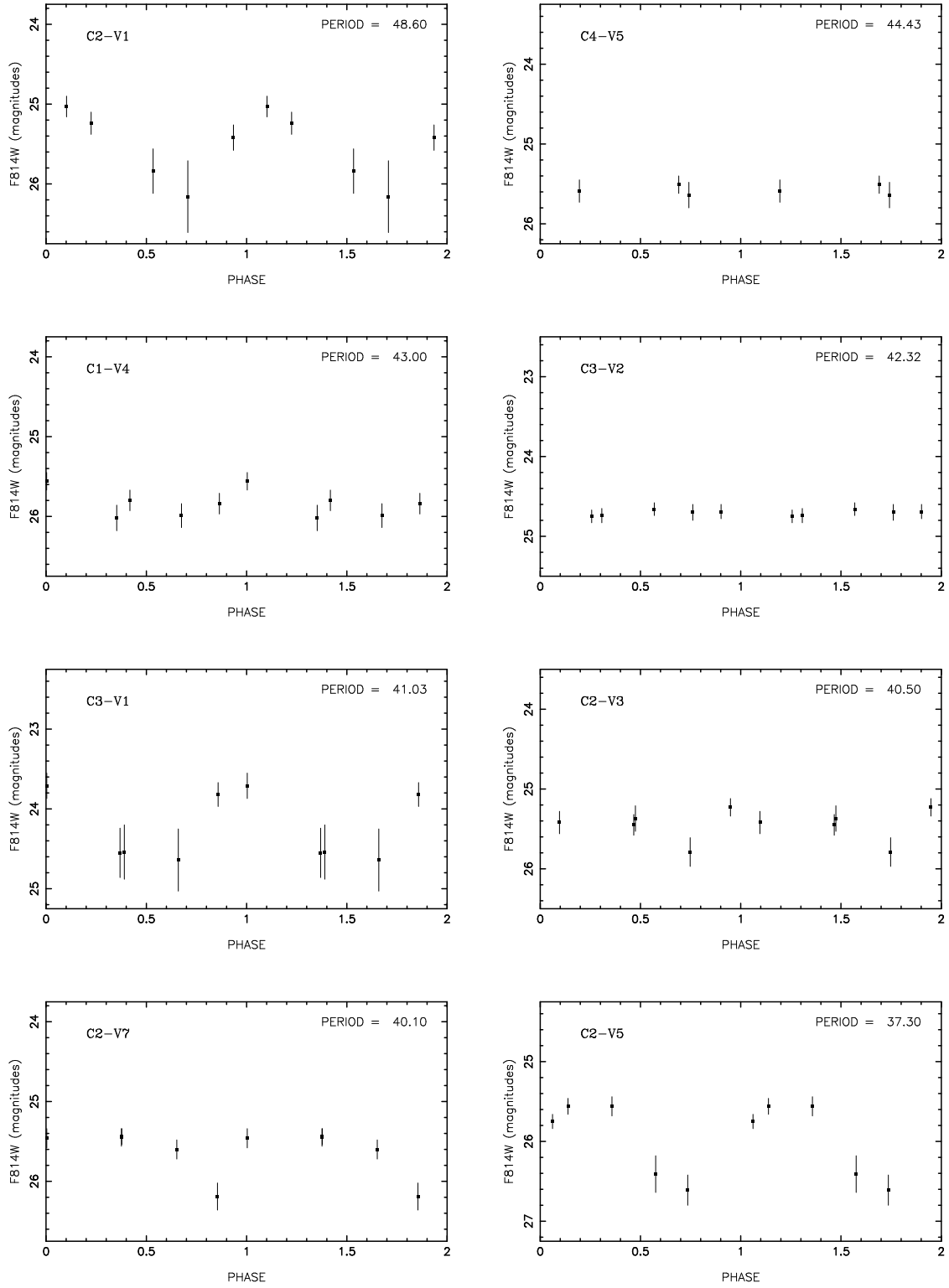
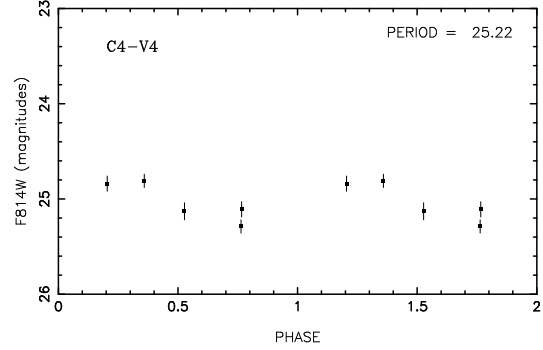
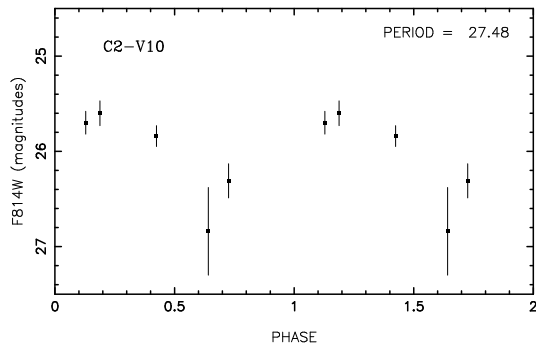
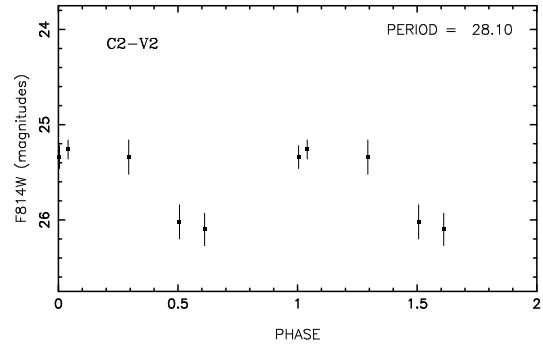
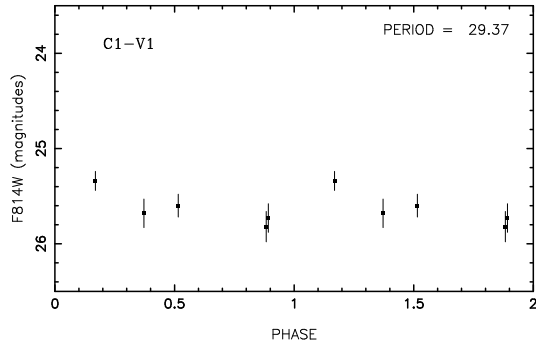
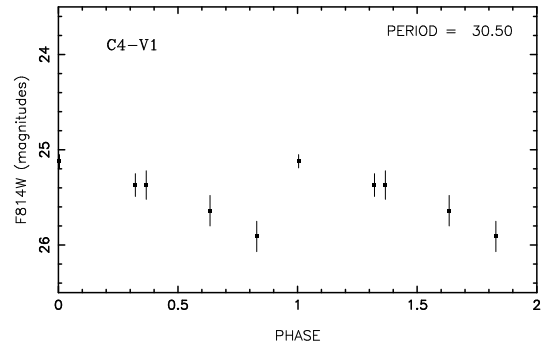
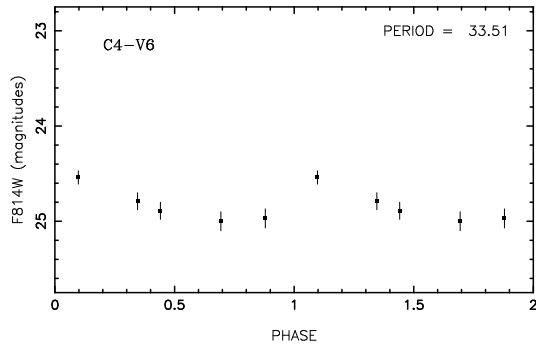
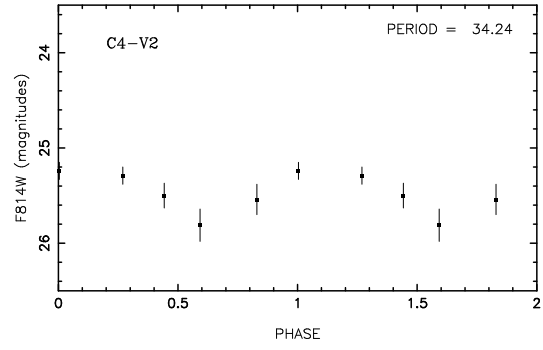
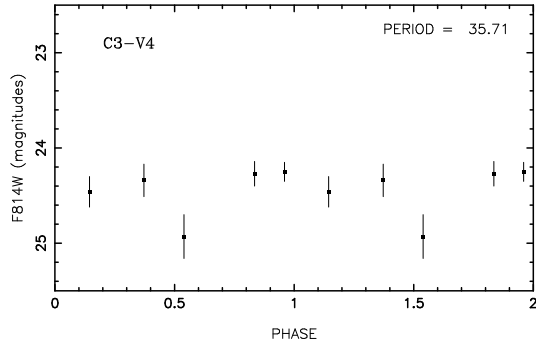
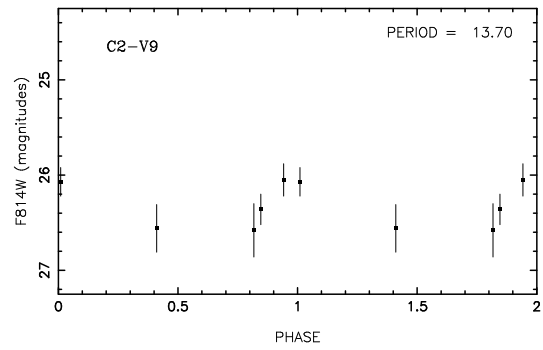
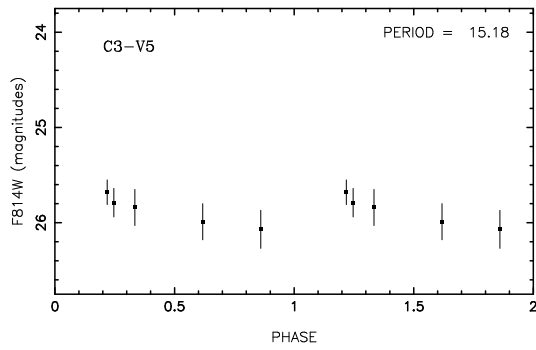
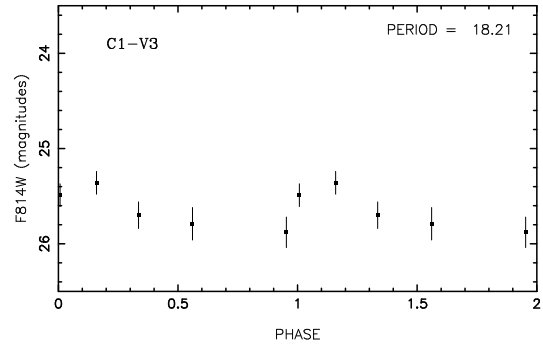
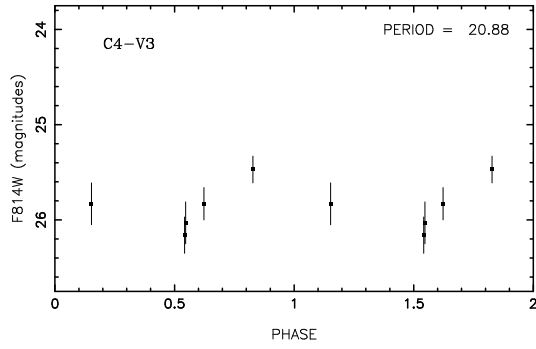
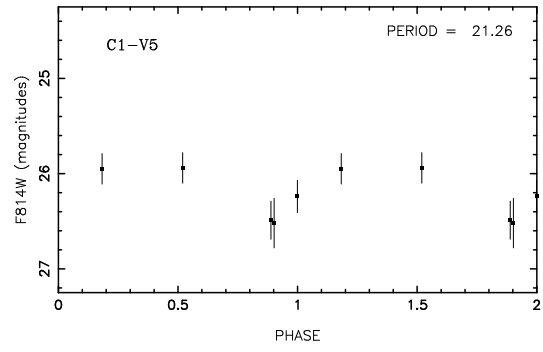
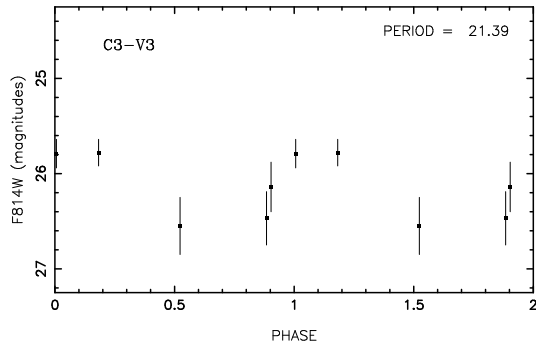
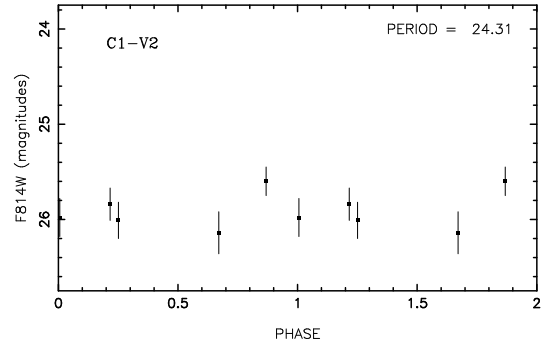
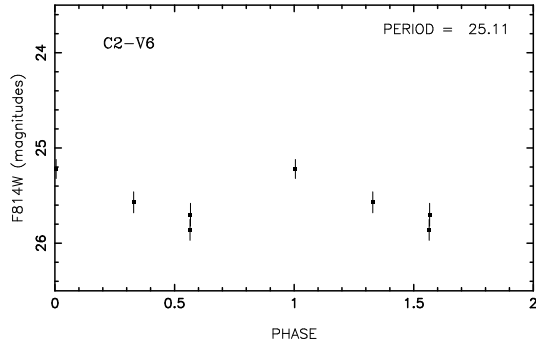
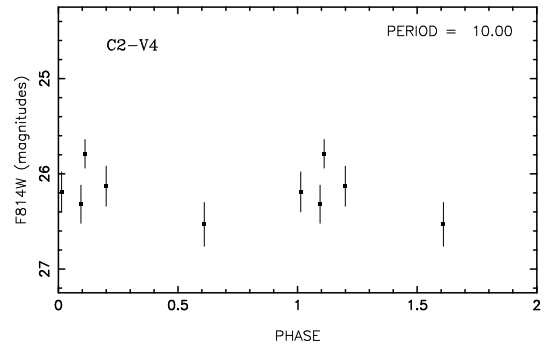
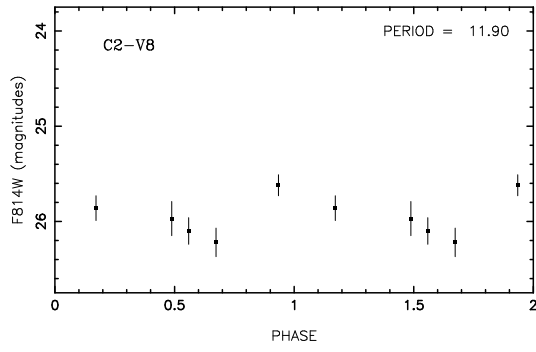


Fig. 4.— Same as Fig. 3 but for the $F814W$ passband, adopting the periods and the phasing used in Fig. 3.







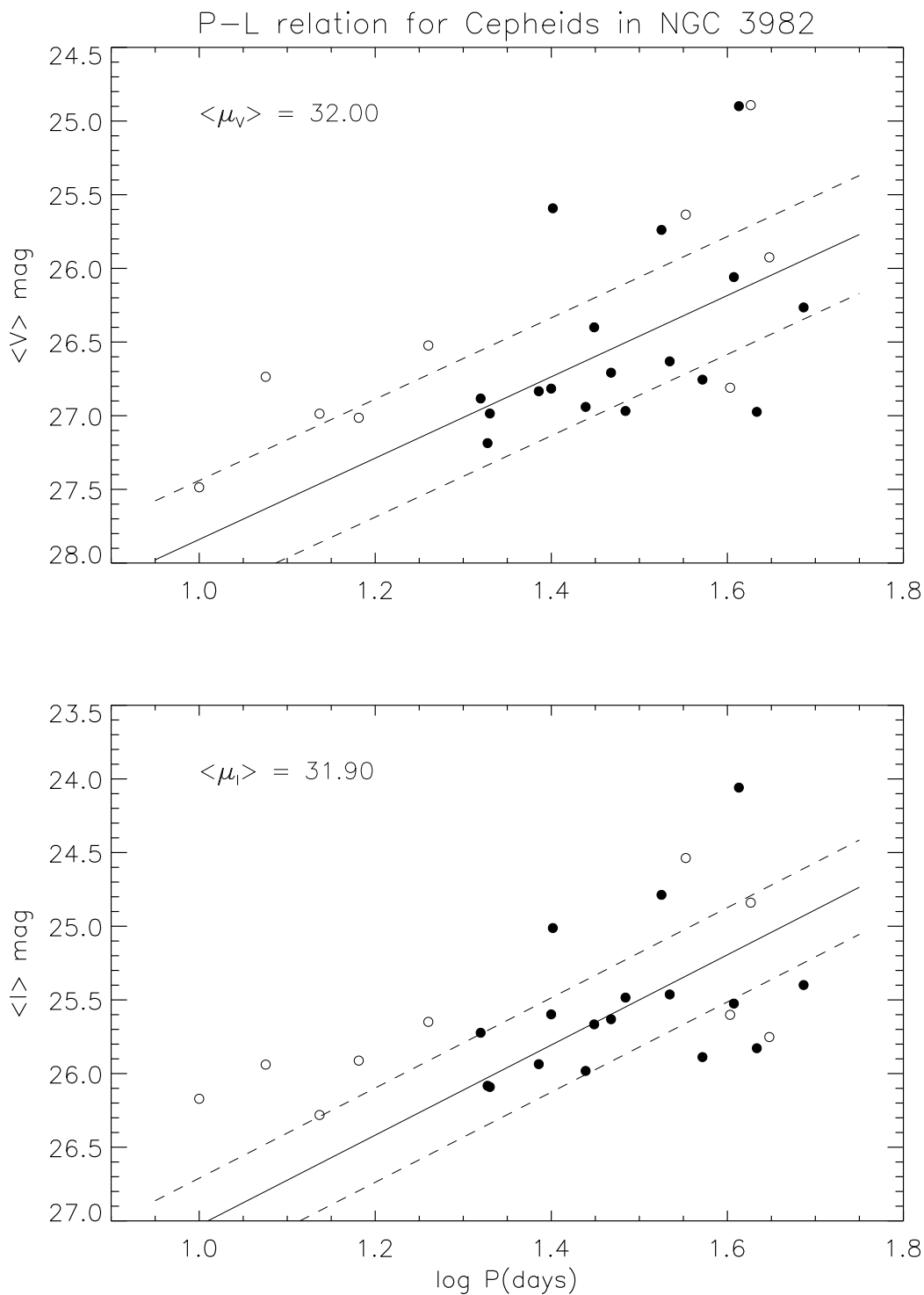


Fig. 5.— The apparent P-L relations in V and I showing all the Cepheid data in Table 4. The solid circles are Cepheids with $P \geq 20^d$ with quality index QI of 3 or better. Open circles are for the remainder of the variables in Table 4. The drawn lines are the adopted P-L relations from Madore & Freedman (1991) in equations (1) and (2) used also in the previous papers of this series. The ridge lines have been put arbitrarily at a modulus of

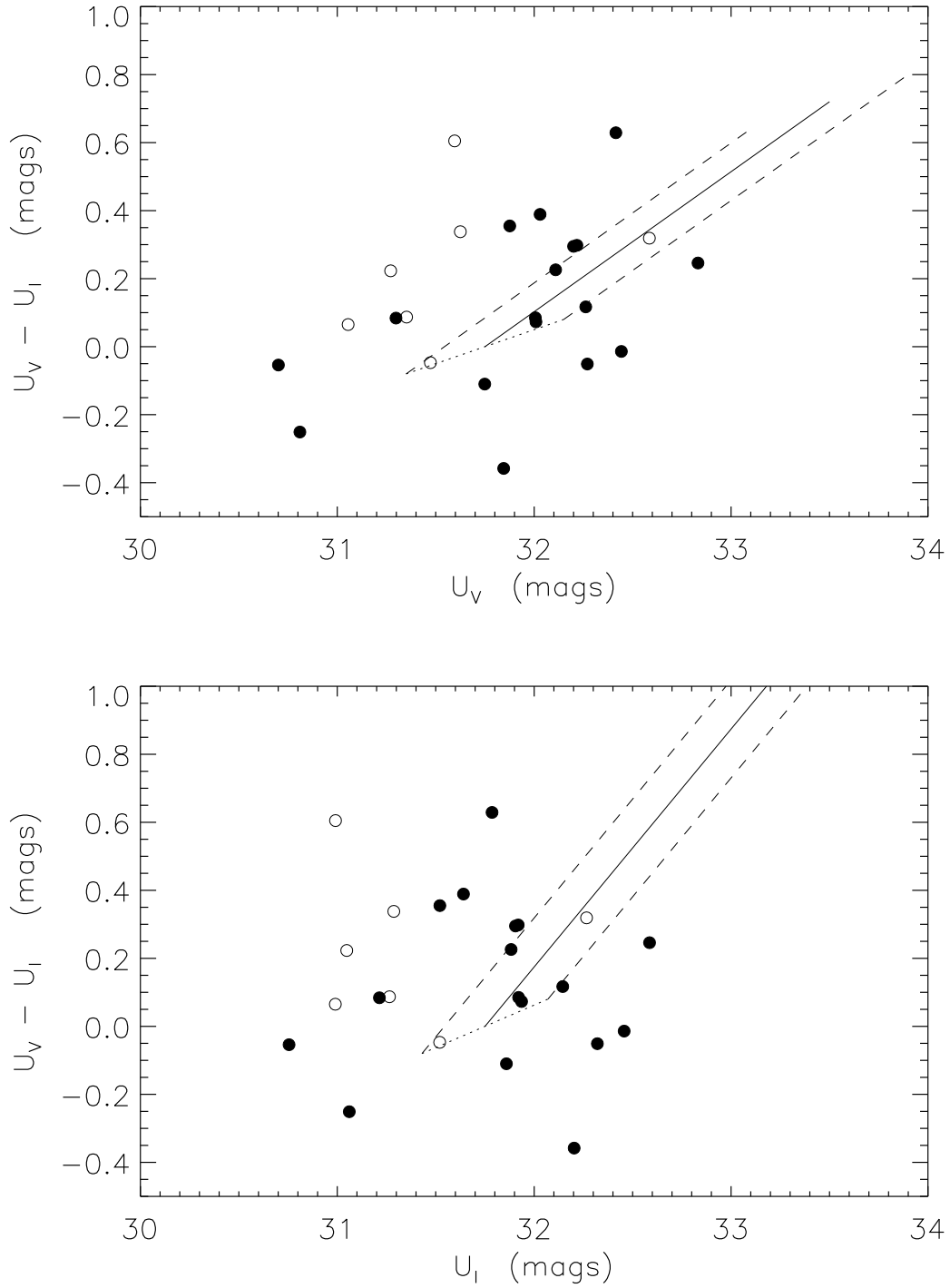


Fig. 6.— Diagnostic diagram for the detection of differential reddening, described in the text. The top panel shows the V -modulus on the abscissa. The lower panel is the same figure, but with the I -modulus on the abscissa.

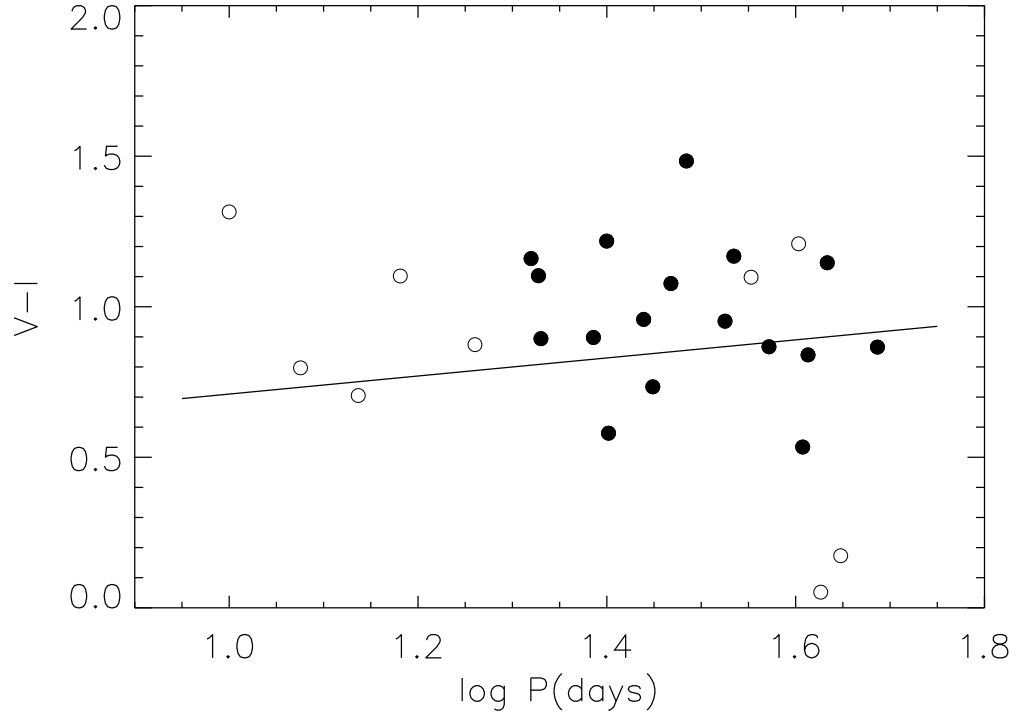


Fig. 7.— The Period Color Relation in V and I . The observed data are shown, with filled circles indicating Cepheids with $P \geq 20^d$, and $QI \geq 3$. The line shows the fiducial relation for unreddened Cepheids that lie on the ridge line of the P-L relation.

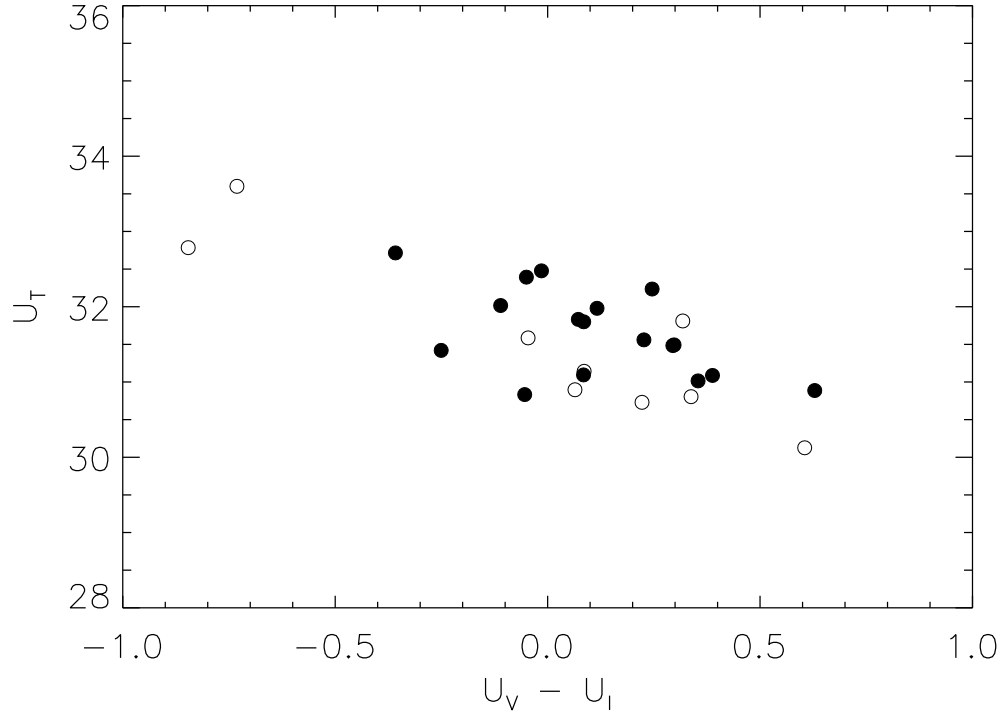


Fig. 8.— Diagram showing the dependence of implied de-reddened modulus as a function of color deviation from the mean P-C relation. The slope is due to misinterpretation of measurement errors as reddening. Outliers with extreme colors are easily identified as being far from the clump of the majority of the objects. Again, filled circles indicate Cepheids with $P \geq 20^d$, and $QI \geq 3$.

Table 1. Journal of Observations.

Data Archive Designation	HJD at Midexposure	Filter
u5ky0101r + ...02r	2451624.018806427	F555W
u5ky0201r + ...02r	2451636.888945493	F555W
u5ky0203r + ...04r	2451637.022626058	F814W
u5ky0301r + ...02r	2451642.923320583	F555W
u5ky0401r + ...02r	2451647.954917874	F555W
u5ky0403r + ...04r	2451648.080265098	F814W
u5ky0501r + ...02r	2451651.255265143	F555W
u5ky0601r + ...02r	2451654.205612403	F555W
u5ky0701r + ...02r	2451656.083042987	F555W
u5ky0703r + ...04r	2451656.214292993	F814W
u5ky0801r + ...02r	2451658.296931908	F555W
u5ky0901r + ...02r	2451662.048668068	F555W
u5ky0903r + ...04r	2451662.180959738	F814W
u5ky1001r + ...02r	2451666.069501458	F555W
u5ky1101r + ...02r	2451672.033737653	F555W
u5ky1201r + ...02r	2451677.060473833	F555W
u5ky1203r + ...04r	2451677.192418277	F814W

All exposures are 2×2500 s

Table 2. Position of the Variable Stars on the Deep-V Image

Variable ID	X-position	Y-position
C1-V1	89.78	397.36
C1-V2	129.86	108.72
C1-V3	378.66	175.47
C1-V4	431.65	239.25
C1-V5	600.06	260.04
C2-V1	80.19	352.03
C2-V2	94.56	536.10
C2-V3	120.03	511.47
C2-V4	213.90	613.04
C2-V5	370.85	507.06
C2-V6	458.11	399.19
C2-V7	509.04	515.58
C2-V8	509.73	151.75
C2-V9	542.60	524.90
C2-V10	568.24	104.44
C3-V1	95.20	352.99
C3-V2	297.30	601.10
C3-V3	400.07	666.87
C3-V4	415.38	294.85
C3-V5	447.77	597.67
C4-V1	118.46	405.86
C4-V2	224.53	214.83
C4-V3	267.86	232.28
C4-V4	416.15	365.64
C4-V5	460.84	249.72
C4-V6	530.88	134.64

Table 3. Photometry of Variable Stars: Magnitudes and Error Estimates

HJD	C1-V1	C1-V2	C1-V3	C1-V4	C1-V5	C2-V1	C2-V2	C2-V3
<i>F555W</i>								
2451624.0188	26.31 0.12	—	26.60 0.12	—	26.21 0.22	25.95 0.10	25.98 0.12	—
2451636.8889	26.83 0.16	27.08 0.24	26.86 0.46	27.14 0.16	26.52 0.12	26.68 0.20	26.96 0.16	26.14 0.08
2451642.9233	27.06 0.17	27.47 0.31	26.44 0.12	27.46 0.23	26.96 0.15	26.57 0.16	27.05 0.19	26.50 0.13
2451647.9549	26.71 0.16	27.26 0.27	26.39 0.10	27.26 0.24	27.80 0.39	25.97 0.10	25.84 0.08	26.45 0.18
2451651.2553	26.10 0.11	26.43 0.12	26.77 0.13	27.23 0.17	27.73 0.25	25.73 0.11	26.11 0.09	26.05 0.12
2451654.2056	26.34 0.13	26.62 0.18	26.97 0.16	27.05 0.14	27.46 0.20	25.98 0.11	26.24 0.09	25.74 0.08
2451656.0830	26.67 0.28	26.13 0.09	26.12 0.12	26.84 0.12	28.05 0.29	25.94 0.10	26.55 0.13	25.70 0.08
2451658.2969	26.53 0.12	26.53 0.12	26.30 0.11	26.55 0.10	26.42 0.11	25.88 0.12	26.43 0.10	25.63 0.08
2451662.0487	26.68 0.14	27.12 0.26	26.60 0.16	26.47 0.09	26.71 0.12	26.01 0.16	26.81 0.17	25.80 0.08
2451666.0695	26.88 0.17	27.08 0.22	26.39 0.13	26.73 0.12	27.30 0.21	26.34 0.13	26.96 0.14	25.89 0.09
2451672.0337	27.35 0.26	27.34 0.31	26.80 0.13	26.90 0.13	27.68 0.25	26.41 0.15	25.93 0.14	26.05 0.11
2451677.0605	26.89 0.16	26.33 0.11	26.23 0.09	27.10 0.15	27.88 0.29	26.52 0.16	25.91 0.07	—
<i>F814W</i>								
2451637.0226	25.60 0.12	25.84 0.17	25.88 0.16	25.80 0.13	26.24 0.17	26.16 0.45	26.10 0.17	25.38 0.16
2451648.0803	25.73 0.16	26.14 0.22	25.80 0.17	25.99 0.15	25.94 0.16	25.42 0.16	25.34 0.12	25.80 0.18
2451656.2143	25.34 0.11	25.98 0.20	25.49 0.12	25.84 0.13	26.52 0.26	25.03 0.13	25.34 0.18	25.23 0.11
2451662.1809	25.68 0.16	26.01 0.19	25.70 0.14	25.56 0.11	25.95 0.16	25.24 0.14	26.02 0.18	25.42 0.14
2451677.1924	25.82 0.16	25.60 0.15	25.36 0.12	26.02 0.16	26.49 0.20	25.84 0.28	25.26 0.10	25.45 0.13
HJD	C2-V4	C2-V5	C2-V6	C2-V7	C2-V8	C2-V9	C2-V10	C3-V1
<i>F555W</i>								
2451624.0188	27.57 0.20	27.23 0.24	26.93 0.16	26.34 0.10	—	26.72 0.14	—	25.32 0.20
2451636.8889	27.36 0.23	26.42 0.09	26.74 0.14	26.67 0.11	27.03 0.12	26.30 0.09	27.26 0.20	25.03 0.16
2451642.9233	27.83 0.26	26.44 0.10	27.19 0.18	27.13 0.20	26.60 0.13	26.98 0.12	27.30 0.20	25.02 0.14
2451647.9549	27.23 0.19	26.76 0.11	25.78 0.18	27.41 0.17	27.08 0.18	27.05 0.15	26.77 0.12	25.32 0.20
2451651.2553	27.31 0.22	26.92 0.13	26.39 0.10	27.33 0.20	26.56 0.09	26.55 0.08	26.80 0.17	25.17 0.16
2451654.2056	28.02 0.38	26.92 0.18	26.58 0.11	27.32 0.17	26.48 0.10	27.09 0.17	26.92 0.15	24.76 0.15
2451656.0830	25.27 0.14	27.27 0.20	26.67 0.14	27.05 0.15	26.51 0.11	27.15 0.19	26.57 0.16	24.53 0.10
2451658.2969	27.21 0.21	27.22 0.19	26.72 0.12	27.10 0.16	26.97 0.16	27.23 0.17	26.91 0.15	24.66 0.15
2451662.0487	27.65 0.28	27.80 0.29	27.01 0.13	26.27 0.07	26.82 0.14	27.47 0.23	27.10 0.15	24.39 0.09
2451666.0695	27.64 0.28	26.89 0.11	26.88 0.13	26.30 0.13	26.45 0.11	26.84 0.13	27.30 0.22	24.61 0.11
2451672.0337	27.28 0.19	26.19 0.07	27.31 0.19	26.46 0.10	27.31 0.19	27.72 0.24	26.51 0.15	24.90 0.16
2451677.0605	27.17 0.16	26.39 0.08	26.01 0.06	26.85 0.14	26.46 0.11	26.35 0.07	26.66 0.14	24.94 0.14
<i>F814W</i>								
2451637.0226	26.32 0.20	25.75 0.09	25.86 0.11	25.45 0.11	26.10 0.14	26.07 0.15	26.31 0.18	24.55 0.34
2451648.0803	26.13 0.21	25.56 0.12	25.22 0.10	25.60 0.12	25.97 0.18	26.58 0.28	25.70 0.12	24.64 0.39
2451656.2143	26.19 0.21	26.41 0.23	25.57 0.11	26.19 0.17	25.86 0.13	26.56 0.25	25.84 0.11	23.82 0.15
2451662.1809	26.53 0.23	26.61 0.19	25.70 0.12	25.46 0.12	26.22 0.15	26.36 0.16	26.84 0.46	23.71 0.16
2451677.1924	25.80 0.16	25.56 0.10	-4.99 0.05	25.44 0.10	25.62 0.11	26.05 0.17	25.60 0.13	24.55 0.31
HJD	C3-V2	C3-V3	C3-V4	C3-V5	C4-V1	C4-V2	C4-V3	C4-V4
<i>F555W</i>								
2451624.0188	24.68 0.12	27.12 0.23	25.51 0.18	27.64 0.31	—	26.10 0.09	26.38 0.10	25.31 0.05
2451636.8889	24.81 0.05	26.26 0.11	25.30 0.15	27.26 0.23	26.47 0.14	26.63 0.14	26.99 0.17	25.80 0.07
2451642.9233	24.86 0.05	26.80 0.15	25.30 0.15	26.30 0.14	26.80 0.14	26.91 0.19	26.49 0.13	25.19 0.04
2451647.9549	24.95 0.05	27.59 0.36	25.52 0.17	26.92 0.20	26.99 0.17	27.18 0.26	26.70 0.15	25.40 0.06
2451651.2553	24.88 0.05	27.20 0.19	25.61 0.19	26.88 0.13	—	27.25 0.26	27.27 0.22	25.38 0.06
2451654.2056	24.98 0.05	27.34 0.29	25.63 0.20	—	27.21 0.20	27.31 0.26	27.68 0.38	—

Table 3—Continued

2451656.0830	24.96 0.05	26.82 0.19	25.68 0.22	27.38 0.23	27.28 0.22	27.15 0.24	27.30 0.25	25.66 0.06
2451658.2969	25.01 0.05	26.68 0.13	25.97 0.28	26.71 0.15	27.30 0.19	26.03 0.08	27.08 0.18	25.89 0.07
2451662.0487	24.92 0.04	26.62 0.13	25.71 0.22	26.72 0.13	27.26 0.24	26.01 0.09	26.63 0.12	25.88 0.07
2451666.0695	24.91 0.05	26.84 0.16	26.01 0.27	—	26.73 0.14	26.23 0.14	26.45 0.14	25.75 0.06
2451672.0337	24.68 0.04	27.36 0.23	25.76 0.20	27.05 0.22	26.65 0.16	26.70 0.13	27.20 0.19	25.38 0.05
2451677.0605	24.74 0.04	27.35 0.22	25.39 0.16	26.83 0.16	26.80 0.19	26.81 0.16	26.84 0.16	25.60 0.05
<i>F814W</i>								
2451637.0226	24.74 0.10	25.80 0.15	24.27 0.13	25.99 0.19	25.12 0.07	25.30 0.09	25.83 0.17	25.11 0.08
2451648.0803	24.66 0.09	26.55 0.30	24.46 0.16	25.84 0.19	25.38 0.15	25.81 0.17	25.83 0.22	24.84 0.08
2451656.2143	24.70 0.11	26.14 0.26	24.34 0.17	26.07 0.20	25.64 0.16	25.55 0.16	26.16 0.19	25.13 0.09
2451662.1809	24.69 0.10	25.78 0.14	24.93 0.23	25.80 0.15	25.91 0.16	25.24 0.09	25.47 0.14	25.30 0.07
2451677.1924	24.75 0.09	26.47 0.28	24.25 0.10	25.68 0.13	25.38 0.12	25.50 0.13	26.03 0.22	24.81 0.07
HJD	C4-V5	C4-V6						
<i>F555W</i>								
2451624.0188	26.06 0.09	26.66 0.24						
2451636.8889	25.63 0.10	25.38 0.10						
2451642.9233	25.62 0.21	25.64 0.10						
2451647.9549	25.56 0.10	25.97 0.12						
2451651.2553	25.57 0.11	26.06 0.11						
2451654.2056	25.93 0.10	26.19 0.12						
2451656.0830	25.88 0.10	26.35 0.18						
2451658.2969	26.01 0.11	26.20 0.13						
2451662.0487	26.75 0.25	26.14 0.13						
2451666.0695	26.41 0.22	24.84 0.08						
2451672.0337	25.98 0.10	25.56 0.09						
2451677.0605	25.91 0.11	25.82 0.11						
<i>F814W</i>								
2451637.0226	25.64 0.16	24.55 0.07						
2451648.0803	—	24.89 0.09						
2451656.2143	25.59 0.14	25.00 0.10						
2451662.1809	—	24.97 0.10						
2451677.1924	25.51 0.12	24.80 0.09						

Table 4. Characteristics of the Cepheids

Object	Period (days)	$\langle V \rangle$	$\sigma_{\langle V \rangle}$	$\langle I \rangle$	$\sigma_{\langle I \rangle}$	U_V	U_I	U_T	σ_{U_T}	Quality Index
(1)	(2)	(3)	(4)	(5)	(6)	(7)	(8)	(9)	(10)	(11)
C1-V1	29.37	26.71	0.17	25.63	0.16	32.16	31.93	31.61	0.51	5
C1-V2	24.31	26.83	0.22	25.94	0.24	32.06	31.99	31.88	0.71	3
C1-V3	18.21	26.52	0.16	25.65	0.26	31.40	31.31	31.19	0.72	4
C1-V4	43.00	26.97	0.16	25.83	0.21	32.88	32.64	32.28	0.61	4
C1-V5	21.26	27.19	0.24	26.08	0.32	32.25	31.95	31.53	0.88	3
C2-V1	48.60	26.27	0.15	25.40	0.37	32.32	32.37	32.44	0.97	5
C2-V2	28.10	26.40	0.13	25.67	0.17	31.80	31.91	32.07	0.53	5
C2-V3	40.50	26.06	0.11	25.53	0.12	31.89	32.25	32.76	0.42	3
C2-V4	10.00	27.49	0.25	26.17	0.32	31.65	31.04	30.18	0.89	0
C2-V5	37.30	26.76	0.15	25.89	0.38	32.49	32.51	32.53	0.99	4
C2-V6	25.11	26.82	0.14	25.60	0.63	32.08	31.69	31.14	1.56	5
C2-V7	40.10	26.81	0.15	25.60	0.29	32.63	32.32	31.86	0.79	1
C2-V8	11.90	26.74	0.13	25.94	0.20	31.10	31.04	30.95	0.57	4
C2-V9	13.70	26.99	0.16	26.28	0.26	31.52	31.57	31.64	0.73	4
C2-V10	27.48	26.94	0.17	25.98	0.44	32.31	32.19	32.03	1.13	3
C3-V1	41.03	24.90	0.15	24.06	0.46	30.75	30.80	30.88	1.17	5
C3-V2	42.32	24.89	0.06	24.84	0.17	30.78	31.63	32.83	0.49	1
C3-V3	21.39	26.99	0.22	26.09	0.34	32.06	31.98	31.85	0.92	5
C3-V4	35.71	25.64	0.20	24.54	0.23	31.32	31.10	30.78	0.68	0
C3-V5	15.18	27.01	0.20	25.91	0.14	31.67	31.34	30.85	0.50	3
C4-V1	30.50	26.97	0.18	25.48	0.11	32.47	31.84	30.94	0.46	5
C4-V2	34.24	26.63	0.19	25.46	0.26	32.27	31.97	31.54	0.73	5
C4-V3	20.88	26.88	0.20	25.72	0.18	31.93	31.57	31.06	0.59	3
C4-V4	25.22	25.59	0.06	25.01	0.14	30.86	31.11	31.47	0.42	3
C4-V5	44.43	25.93	0.15	25.75	0.15	31.87	32.60	33.65	0.49	1
C4-V6	33.51	25.74	0.12	24.79	0.17	31.35	31.26	31.14	0.51	5

Table 5. HSTphot results for Variables found in Common

Object	Period (days)	$\langle V \rangle$	$\sigma_{\langle V \rangle}$	$\langle I \rangle$	$\sigma_{\langle I \rangle}$	Quality Index
(1)	(2)	(3)	(4)	(5)	(6)	(7)
C1-V1	31.05	26.49	0.13	25.44	0.15	4
C1-V2	24.90	26.59	0.14	26.16	0.18	4
C1-V4	37.73	26.77	0.14	25.72	0.16	3
C1-V5	21.83	27.01	0.15	25.99	0.18	3
C2-V2	28.10	26.53	0.19	25.80	0.26	3
C2-V5	37.34	26.72	0.11	25.76	0.14	4
C2-V6	27.96	26.76	0.16	25.55	0.18	4
C2-V7	37.14	26.76	0.15	25.75	0.18	4
C2-V9	13.81	26.93	0.12	26.43	0.18	2
C2-V10	25.97	27.11	0.17	26.11	0.20	3
C3-V3	22.65	26.89	0.22	25.96	0.24	2
C3-V4	32.22	25.28	0.09	24.41	0.12	1
C4-V1	35.80	26.55	0.13	25.37	0.16	4

Table 6. Mean absolute B , V , and I magnitudes of nine SNeIa without and with corrections for decline rate and color

SN (1)	Galaxy (2)	$(m - M)^0$ (3)	M_B^0 (4)	M_V^0 (5)	M_I^0 (6)	Δm_{15} (7)	$(B - V)^0$ (8)	M_B^{corr} (9)	M_V^{corr} (10)	M_I^{corr} (11)
1937C	IC 4182	28.36 (12)	-19.56 (15)	-19.54 (17)	...	0.87 (10)	-0.02	-19.39 (18)	-19.37 (17)	...
1960F	NGC 4496A	31.03 (10)	-19.56 (18)	-19.62 (22)	...	1.06 (12)	0.06	-19.67 (18)	-19.65 (22)	...
1972E	NGC 5253	28.00 (07)	-19.64 (16)	-19.61 (17)	-19.27 (20)	0.87 (10)	-0.03	-19.44 (16)	-19.42 (17)	-19.12 (20)
1974G	NGC 4414	31.46 (17)	-19.67 (34)	-19.69 (27)	...	1.11 (06)	0.02	-19.70 (34)	-19.69 (27)	...
1981B	NGC 4536	31.10 (12)	-19.50 (18)	-19.50 (16)	...	1.10 (07)	0.00	-19.48 (18)	-19.46 (16)	...
1989B	NGC 3627	30.22 (12)	-19.47 (18)	-19.42 (16)	-19.21 (14)	1.31 (07)	-0.05	-19.42 (18)	-19.41 (16)	-19.20 (14)
1990N	NGC 4639	32.03 (22)	-19.39 (26)	-19.41 (24)	-19.14 (23)	1.05 (05)	0.02	-19.39 (26)	-19.38 (24)	-19.02 (23)
1998bu	NGC 3368	30.37 (16)	-19.76 (31)	-19.69 (26)	-19.43 (21)	1.08 (05)	-0.07	-19.56 (31)	-19.55 (36)	-19.31 (21)
1998aq	NGC 3982	31.72 (14)	-19.56 (21)	-19.48 (20)	...	1.12 (03)	-0.08	-19.35 (24)	-19.34 (23)	...
straight mean:			-19.57 (04)	-19.55 (04)	-19.26 (0 6)			-19.49 (04)	-19.47 (04)	-19.16 (06)
weighted mean:			-19.56 (07)	-19.53 (06)	-19.25 (0 9)			-19.47 (07)	-19.46 (06)	-19.19 (09)

This figure "Fig1.jpg" is available in "jpg" format from:

<http://arxiv.org/ps/astro-ph/0107391v1>

This figure "Fig2_1.jpg" is available in "jpg" format from:

<http://arxiv.org/ps/astro-ph/0107391v1>

This figure "Fig2_2.jpg" is available in "jpg" format from:

<http://arxiv.org/ps/astro-ph/0107391v1>

This figure "Fig2_3.jpg" is available in "jpg" format from:

<http://arxiv.org/ps/astro-ph/0107391v1>

This figure "Fig2_4.jpg" is available in "jpg" format from:

<http://arxiv.org/ps/astro-ph/0107391v1>